

A Review of Indoor Millimeter Wave Device-based Localization and Device-free Sensing Technologies

Anish Shastri, Neharika Valecha, *Student Member, IEEE*, Enver Bashirov, *Student Member, IEEE*,
 Harsh Tataria, *Member, IEEE*, Michael Lentmaier, *Senior Member, IEEE*,
 Fredrik Tufvesson, *Fellow, IEEE*, Michele Rossi, *Senior Member, IEEE*,
 and Paolo Casari, *Senior Member, IEEE*

Abstract

The commercial availability of low-cost millimeter-wave (mmWave) communication and radar devices is starting to improve the penetration of such technologies in consumer markets, paving the way for large-scale and dense deployments in fifth-generation (5G)-and-beyond as well as 6G networks. At the same time, pervasive mmWave access will enable device localization and device-free sensing with unprecedented accuracy, especially with respect to sub-6 GHz commercial-grade devices. This paper surveys the state of the art in device-based localization and device-free sensing using mmWave communication and radar devices, with a focus on indoor deployments. We first overview key concepts about mmWave signal propagation and system design. Then, we provide a detailed account of approaches and algorithms for localization and sensing enabled by mmWaves. We consider several dimensions in our analysis, including the main objectives, techniques, and performance of each work, whether each research reached some degree of implementation, and which hardware platforms were used for this purpose. We conclude by discussing that better algorithms for consumer-grade devices, data fusion methods for dense deployments, as well as an educated application of machine learning methods are promising, relevant and timely research directions.

Index Terms

Millimeter waves; propagation characteristics; channel models; communications; localization; sensing; radar; practical constraints;

Manuscript received xxxx xx, xxxx ...

This work received support from the European Commission's Horizon 2020 Framework Programme under the Marie Skłodowska-Curie Action MINTS (GA no. 861222), and from Italian Ministry for Education, University and Research (MIUR) under the "Departments of Excellence" initiative (Law 232/2016).

A. Shastri (email: anish.shastri@unitn.it) and P. Casari (email: paolo.casari@unitn.it) are with the Department of Information Engineering and Computer Science, University of Trento, 38123 Povo (TN), Italy.

N. Valecha (email: neharika.valecha@eit.lth.se), M. Lentmaier (email: michael.lentmaier@eit.lth.se) and F. Tufvesson (email: fredrik.tufvesson@eit.lth.se) are with the Department of Electrical and Information Technology, Lund University, 22100 Lund, Sweden.

E. Bashirov (email: enver.bashirov@dei.unipd.it), and M. Rossi (email: rossi@dei.unipd.it) are with the Department of Information Engineering, University of Padova, 35131 Padova, Italy.

H. Tataria (email: harsh.tataria@ericsson.com) is with Ericsson AB, 22363 Lund, Sweden.

I. INTRODUCTION

MmWave communications in the 28–300 GHz band are looked at with great interest, as they may be able to quench –at least temporarily– the ever-increasing bandwidth requirements of such applications as massive Internet of things (IoT), virtual/augmented reality, mobile cloud services and ubiquitous ultra-high definition multimedia streaming [1]–[3]. This would cover the shortcomings of sub-6 GHz technologies such as WiFi and fourth-generation (4G) cellular networks, which currently cannot support the massive bandwidth and number of users the above applications imply.

The potential of mmWave technology, however, is not limited to higher-rate communications: rather, mmWave devices can become a proxy for high-resolution device-based localization as well as device-free sensing. These capabilities follow from the physics of mmWave propagation. First, the shorter wavelength of mmWave (compared to sub-6 GHz signals) enables higher location estimation accuracy and lower location error bounds [4], [5]. Second, mmWaves have well-known and peculiar propagation characteristics [6], [7] which naturally enable better spatial scanning resolution. For example, mmWaves propagate quasi-optically, meaning that a line-of-sight (LoS) multipath component (MPC) is predominant over non line-of-sight (NLoS) contributions to the received signal [8]. Scattering also has a limited impact off typical non-rough reflecting surfaces such as walls, furniture, metal plates as well as glass layers [9], [10].

Another consequence of mmWave propagation is that mmWave signals undergo much higher path loss with respect to microwaves. To compensate for this attenuation, and still enable long-reach wireless links, mmWave devices resort to large or massive antenna arrays. Via beamforming, they can focus their transmitted energy towards a confined portion of the 3D space, and thus achieve greater directionality. While this requires specific protocols for initial access [11]–[13] and beam training such as the IEEE 802.11ad [14], [15] and 802.11ay [16], [17] standards, it also means that a reduced amount of power is typically directed towards secondary multipath components. In addition with the quasi-optical propagation patterns discussed above, the main consequence is that the received angular spectrum of a mmWave signal is sparse: in typical conditions, one can identify one LoS MPC along with a number of NLoS MPCs corresponding to signal reflections off the surrounding environment. The above features of mmWave communications have significant implications for localization and sensing. For example, being able to separate MPCs in the angular domain enables angle-based localization schemes that are not normally used in sub-6 GHz systems due to limited angular resolution when using small antenna arrays. Fingerprinting-based algorithms can also be enhanced by incorporating angle-based features to improve location discrimination. From the point of view of device-free sensing, mmWave propagation also implies typically clearer reflections off sensed targets and parts thereof. For example, a) quasi-optical mmWave propagation along with b) the large mmWave bandwidth available at typical mmWave radar frequencies respectively imply that reflections off targets are usually separate in the a) angle and b) time domains. This makes it possible to measure features that point to each reflection’s movement velocity (e.g., the Doppler shift) and use this data to precisely localize and identify different targets.

In this paper, we focus on indoor mmWave device-based localization and device-free sensing, and provide a comprehensive review of approaches, technologies, schemes and algorithms to estimate a device or object’s location

in an indoor environment. The objective of our survey is to shed light on indoor applications of localization and sensing using mmWave signals. For this, we start with an overview that touches on mmWave signal structure and propagation characteristics that make this domain unique with respect to other radio communication and sensing technologies. We consider practical constraints that define the applicability of algorithms and processing schemes to mmWave devices operating indoors. We then delve into a detailed description of device-based indoor localization algorithms, explaining the main localization techniques employed in the literature, and how they are practically implemented in real mmWave hardware whenever available. For device-free sensing, we list a number of relevant applications and technologies that leverage mmWave hardware and signals to detect, localize and track targets indoors, as well as to specifically identify features related to sub-sections of a target (e.g., a part of the human body). Because these device-free approaches are mainly based on mmWave radar devices, we will briefly discuss how mmWave radar bands are being standardized for different applications.

A. Differences with respect to previous surveys

Localization and sensing are topics of great interest for both current and future-generation wireless communication system engineering. The research on these topics has proceeded at a steady pace, considering aspects as diverse as localization techniques, heterogeneous technologies, different scenarios, and different kinds interactions between the device to be localized and the location server, among others. Several surveys cover these aspects, typically for sub-6 GHz technologies. For example, Zafari et al. [18] and Geok et al. [19] focus on localization techniques for wireless systems in general, and cover heterogeneous technologies. These works only tangentially consider mmWaves, and instead survey geometric and signal processing-based localization methods for sub-6 GHz systems. Ngamakeur et al. [20] delve into device-free sensing of different human signatures using sub-6 GHz technologies indoors. Here, the focus is on the localization, tracking and identification of multiple subjects using Wi-Fi and other kinds of wireless sensors.

By leveraging similar technologies, Singh et al. [21] consider techniques and algorithms to localize IoT devices indoors. In this case, the focus of the survey is on a specific source of location information (WiFi received signal strength fingerprints) and on how machine learning works when applied to such datasets. By expanding into the concept of smart world, the work in [22] also surveys how sub-6 GHz technologies can help improve a variety of services via data collection and system automation using active and passive sensing techniques. Finally, the work in [23] touches on aspects related to the modeling and estimation of wireless channels in 5G cellular systems. While the work touches on localization, the covered techniques apply to outdoor cellular systems, and can thus leverage the density and much higher computational power of their hardware.

Unlike our survey, none of the above works targets millimeter wave device-based and device-free indoor localization. This area is characterized by several interesting research works to date, but remains a very hot topic due to the inception of mmWave coverage for future fifth-generation networks as well as wireless (indoor) local-area networks. The objective of our survey is to cover the most significant work in this area, while giving a comprehensive view of unsolved challenges and open research avenues.

Note that, in our survey, we are *not* seeking an analysis of the limits of mmWave localization and sensing technology based on purely theoretical arguments, or an operational description of well-known geometric localization algorithms, or even a coverage of the integration between mmWave communications and 5G, beyond-5G, and future 6G networks. These are related yet tangential topics for which we rather refer the interested reader to one of the several excellent surveys that touch on these aspects, e.g., [23]–[27].

B. Outline and organization of the manuscript

The remainder of this paper expresses three purposes: to cover the characteristics of mmWave propagation and communication/sensing hardware that impacts localization and sensing performance, including standardization efforts (Sections II through IV); to detail the state of the art in device-based mmWave localization (Section V) and in device-free mmWave sensing (Section VI); and finally to discuss our findings, discuss promising research avenues, and draw concluding remarks (Sections VII and VIII).

In particular, Sections V and VI constitute the core of our technological survey. Section V discusses device-based localization algorithms for indoor environments, whereas Section VI presents several approaches for radar-based device-free localization. Each section is organized to first present the section topic, and then add progressively more details related to the typical techniques appropriate for each section, the hardware typically used in testbeds, and the description of each surveyed approach. Each section includes summary tables to help the reader navigate the contents and extract key information. Both Sections V and VI end with a summary of the most relevant aspects and findings.

II. INFLUENCE OF MMWAVE CHANNELS

A. Impact of mmWave frequencies on propagation conditions

The propagation of a wave through any medium depends on its frequency: this basic property helps us predict the behaviour of the channel for different carrier frequencies. When it comes to mmWave, considering the Friis equation under the assumption that the antenna gain G at both link ends is frequency-independent (by reducing the antenna aperture), the free space path loss increases with the square of the carrier frequency f . On the contrary, assuming a constant physical area A at both the transmitter (TX) and the receiver (RX), the antenna gains $G = A(4\pi/\lambda)^2$ increase on both sides, and thus the overall path loss *decreases* quadratically with increasing frequency f [28]. Specular reflections for dielectric halfspaces (e.g., ground reflections) depend on frequency as long as the dielectric constant is itself a function of frequency. For reflections at a dielectric layer (e.g., building walls) the specular reflections depend on the electrical thickness of the wall, which in turn is also a function of frequency. Interestingly, we have no evidence that the reflection coefficient varies with frequency, although the transmission power decreases uniformly with increasing frequency due to the skin effect in lossy media [29].

Two effects that have gained spotlight with the increased interest in the mmWave band are diffraction and diffuse scattering. The former reduces noticeably at high frequencies, and larger objects lead to “sharp” shadows. The latter effect is more significant as the surface roughness becomes comparable to mmWave wavelengths. As the surface roughness increases, the objects behave like a Lambertian radiator, which scatters the radiation. Foliage has

a similar effect as scattering; with the decreasing wavelength relative to the size of the leaves, we observe more diffused scattering and less penetration.

Channel models used for localization need to account for the above mentioned phenomena, and are often based on ray tracing or cluster-based modeling with some geometry-based stochastic channel model (GSCM). Moreover, for ray tracing approaches, high-resolution environment information is needed to account for such surface roughness, as different materials have different properties (e.g., glass windows vs. concrete walls). These effects also depend on the environment: the high concrete walls and glass surfaces of the urban areas lead to different propagation conditions, compared to the greener suburban areas with, e.g., stucco exteriors and shorter walls.

B. Measurement techniques and results

Measuring the characteristics of mmWave channels is complicated due to the cost of the equipment needed, as well as the sensitivity to non-idealities. Due to the short wavelength, the impact of *phase noise*, as well as *errors in distance* between antenna elements of an array, is an order of magnitude larger than for conventional sub-6 GHz systems. Similarly, the cost and energy consumption of up/down-conversion chains, in particular of the front-end mixed signal circuitry in analog-to-digital and digital-to-analog converters (ADCs/DACs) as well as power amplifiers (PAs) becomes of paramount importance. For up-to-Gbit/s sampling rates (as often required by best-in-class channel sounding), 12-15 bit resolution is required.

To penetrate larger distances (and thus to maximize the forward link gain), PAs typically need to operate with 6-10 dB backoff power efficiency and need to be continuously driven close to their 1 dB compression point limits. For these reasons, the vast majority of channel sounders either lack high directional resolution (i.e., with either directional or omnidirectional antennas at both link ends, but in any case the angular distribution of the radiation was not measured) [28] or directional resolution was largely obtained by mechanically rotating a directional (horn) antenna, and measuring the impulse responses for each horn orientation. Here, the beamwidth of the antenna essentially determines the angular resolution of the measurement, e.g., [30], [31]. This is in contrast to sub-6 GHz measurements, where directional evaluations using switched arrays in conjunction with super-resolution techniques provide accurate directional information. Some improvements in this have been observed by the channel sounding systems proposed by [32]. The common theme of all these solutions is the *phased array* nature of radio frequency (RF) front-ends with single or multiple RF up/down-conversion chains.

For indoor measurements, several studies employed rotating horn antennas or virtual arrays (in combination with vector network analyzers to provide phase stability). In the latter case, the evaluation of the measurements can proceed using super-resolution algorithms such as space-alternating generalized expectation maximization (SAGE) [33] and RIMAX [34]. The same can be achieved with electronically-switched horn arrays [31], [35]. This makes it possible to evaluate the number of MPCs and obtain insight on intra-cluster characteristics.

1) *Key outdoor results:* A key result of outdoor measurements is that the path loss coefficient at mmWave frequencies is similar to that of sub-6 GHz spectrum in many situations. Specifically, for LoS scenarios, the path loss coefficient is in the range of 1.6-2.1 (it would be 2 for pure free-space propagation). For NLoS scenarios, the path loss coefficient is typically between 2.5 and 5 (e.g., [31], [36]). There often is no strong frequency dependence

beyond the f^2 dependence of free-space path loss [29], [37]. However, the variance of the path loss around the distance-dependent mean is considerably larger at mmWave frequencies. Thus the probability of outage is higher, and requires appropriate countermeasures [38]. The standard deviation of the path loss is also a strong function of distance, increasing from typically 5-10 dB at 30 m to more than 20 dB at 200 m [39]. Recent work shows this effect may not actually be due to shadowing, but rather that different streets (and different cells) have different path loss coefficients (ranging from almost 0 to more than 10), so that very different power levels are experienced in different streets [40].

A large range of delay spreads have been measured or simulated by ray tracing in outdoor environments [36], [41]–[44]. Astonishingly, the reduction of the delay spread by beamforming, while noticeable, is not overwhelming: a factor of 2 or 3 is typical [45]. Another important issue is the frequency dependence of the delay spread: various papers in the literature show different results, which are strongly related to the use of different dynamic ranges and post-processing methods. This throws in doubt whether root mean square (RMS) delay spread is the best measure for quantifying delay dispersion for these systems. Rather, delay windows (defined as the time delay interval that contains some fraction x of the energy of the power delay profile), might be better suited.

Moreover, the angular dispersion characteristics are critical because they determine the type of beamforming, and the achievable gain. For many outdoor environments, the RMS angular spread at the base station (BS) is on the order of 10° , and only a single cluster can be observed, e.g., [46]–[48]. However, a number of measurements have observed multiple clusters, which provides the possibility of beam-switching to enhance robustness, when the main direction becomes blocked by a moving obstacle. At the user equipment (UE), angular spreads are considerably larger, often in the range 30 – 70° [36], [49]. While ray tracing generally predicts the angular spreads at the BS well, it tends to significantly underestimate the angular spreads at the UE, because many scattering objects such as street signs, parked cars, etc., are not included in geographic databases used for ray tracers [50].

For fixed wireless access scenarios, the temporal Rice factors describe the relative importance of time variations compared to the fixed component. Rice factors of about 20 dB at shorter distances, decreasing to a few dBs at large distances, have also been measured. This indicates the importance of compensating for and/or exploiting temporal fading even in these scenarios [51].

2) *Key indoor results:* Results in indoor environments are largely drawn from office environments and hotspots such as lobbies, malls, train stations, etc. The path loss coefficient is in the order of 2-3 in NLoS scenarios, and 1.2-2 in LoS scenarios [33], [52]; some results in office environments suggest a two-slope model, as propagation to larger distances involves either penetration through multiple walls, or at least one diffraction [53]. Again, these values are similar to what is observed at lower frequencies, but with a higher outage probability (due to shadowing by humans blocking the LoS path, as well as highly absorbing steel/concrete walls). The frequency dependence of the path loss is more pronounced in indoor environments than outdoors: f^k with $k \approx 2.5$ was observed in [54]. Delay spread values in offices are often less than 5 ns in LoS conditions, and 10–50 ns in NLoS conditions [52], [55], [56]. For hotspots, the NLoS delay spreads can range up to 150 ns [35].

The power delay profile is often described via a Saleh-Valenzuela (SV) model, with the key difference that the power-delay profile (PDP) of each cluster is not a single-exponential decay and zero otherwise (when the

cluster starts at $t = 0$), but rather exhibits pre-and post-cursors of the strongest component [57]. The directional characteristics can be described by an extended SV model, with azimuth angles of the cluster centers typically described as uniform and intra-cluster azimuth dispersion with a Laplacian distribution, while elevation angles also have a Laplacian distribution with a spread of about 5° [58]. Another interesting property is the number of MPCs observed in the measurements. High resolution evaluations tend to find a larger number of MPCs and clusters than non-directional or rotating-horn measurements [35], [59]. Also, the study in [60] used Fourier beamforming with a very large virtual array ($25 \times 25 \times 25$ elements) and found that a significant part of the multipath energy is diffuse (or can be explained through a large number of discrete components), in contrast to the common assumption of sparsity in mmWave channels.

C. Models for mmWave channels

Because mmWave propagation channels differ from microwave channels, we need to redefine or rather add certain parameters for mmWave channel modeling. As mentioned in [61], mmWave channels require 3D modeling of azimuth as well as elevation spreads, inclusion of temporal/spatial/frequency consistency and multipath cluster based modeling. These have further impact when we consider positioning and localization. Prevalent models for mmWave are GSCMs that imitate the propagation environment with stochastic processes, and create a 3D map. To correctly reproduce the wireless environment, parameter values need to be extracted from the channel impulse response of real time measurements done using a channel sounder. The Third-generation partnership project (3GPP) defined different environments for mmWave channel modeling, these include Urban Macro, Urban Micro, Indoor Office and Rural Macro. Several outdoor and indoor measurements are available, but for this paper we compare large-scale parameter values for an indoor office scenario listed in Table I.

Prominent channel models have been developed for the above mentioned scenarios based on measurements done in each of them. Some key results have already been discussed, but we also observe that cluster-based multipath channel components have been modelled, in order to specifically account for an indoor office environment. Also, as can be seen from the table, the angular spread is no longer limited to the azimuth plane.

1) Static vs. dynamic modeling: Due to the high frequency and thus higher path loss, there is significant deterioration when the UE is stationary and more so when the UE is moving or is in a high movement zone and transitions from a LoS to NLoS scenario. This requires the dynamic modeling of the communication channel, as the moving objects in the vicinity also act as random blocking obstacles. The BS needs to transmit training beams more frequently so as to update the angle of departure (AoD)/angle of arrival (AoA) estimates, since the location of UE changes over time, and slight errors in the orientation of the beams can lead to significant performance loss [67]. So far, we have considered a fixed BS and slow moving UE, but with 5G and vehicle-to-everything (V2X) communications we expect high mobility scenarios. Most mmWave channel models, are still defined only for a fixed BS, but have added support for dynamic modeling scenarios for V2X.

2) Blockage: The effect of any obstacles such as human bodies, walls, foliage etc is higher for mmWaves as they cannot penetrate them. Thus, these blockages need to be modelled in the link budget itself. The effect of the blockage is not only on the total received power but also on the angle or power of multipath due to varying

TABLE I
SUMMARY OF CHANNEL MODELS AND THEIR SPATIAL PARAMETER VALUES

Parameter		mmWave Channel Models				
		3GPP [62] / ITU-R [63]	COST IRACON [64]	METIS [57]	QuaDRiGa [65]	NYUSIM [66]
f (GHz)		6	2.6	0.45-63	5.4	28
Type		2D GSCM	GSCM	3D Map-based & GSCM	3D GSCM	TCSL
K- factor	μ_K	7	N/A	7.9	-1.6	N/A
	σ_K	4	N/A	6	2.7	N/A
Delay Spread	μ_{DS}	-7.7	1.07	-7.42	-7.22	2.7
	σ_{DS}	0.18	0.93	0.32	0.08	1.4
AOA Spread	μ_{ASA}	1.62	3.94	1.65	1.67	19.3
	σ_{ASA}	0.22	3.91	0.47	0.15	14.5
AOD Spread	μ_{ASD}	1.60	0.71	1.64	1.54	23.5
	σ_{ASD}	0.18	0.59	0.43	0.1	16.0
ZOA Spread	μ_{ZSA}	1.22	3.73	1.28	1.61	7.4
	σ_{ZSA}	0.297	2.11	0.26	0.07	3.8
ZOD Spread	μ_{ZSD}	N/A	1.95	1.31	1.17	-7.3
	σ_{ZSD}	N/A	1.80	0.31	0.07	3.8
XPR (dB)	μ_{XPR}	11	15.59	29	13	N/A
	σ_{XPR}	4	10.39	6.5	1.6	N/A
Shadow fading	μ_{PL}	47.9	N/A	N/A	36.1	N/A
	σ_{PL}	3	N/A	3	1.6	N/A

sizes, positions and directions of the blocking object/human. Localizing the position of the UE with respect to these blockage sources becomes onerous especially in a dynamic setting.

3) *Spatial consistency and clusters*: A new, previously unexplored requirement was added to 3GPP Release 14 [62]. When mmWave communications take place through narrow antenna radiation beams, the channel characteristics become highly correlated, especially when two UEs are close and see the same BS. Also, for applications related to V2X communications, it is paramount that the channel evolves smoothly without discontinuities during mobility [68].

4) *Polarization*: The radiation pattern of each antenna element of an array extends over both the azimuthal plane and the elevation plane, and should be separately modelled for directional performance gains. Moreover, as we consider indoor scenarios with higher number of reflections, the polarization properties of the multipath components also come into play.

5) *Large bandwidth and large antenna arrays*: Antenna arrays that are larger in size and also massive in the number of antenna elements are needed at mmWave, thus high resolution channel modeling includes propagation patterns both in the angular domain and in the delay domain. This is done by accurately modeling the higher number of multipath components and their AoA/AoD. Antenna elements in azimuth and elevation plane both need to be evaluated to consider all possible array structures (planar array, rectangular array, cylindrical array). Fig. 1 depicts an antenna array panel used for 3GPP/International telecommunication union – radiocommunication Sector (ITU-R)

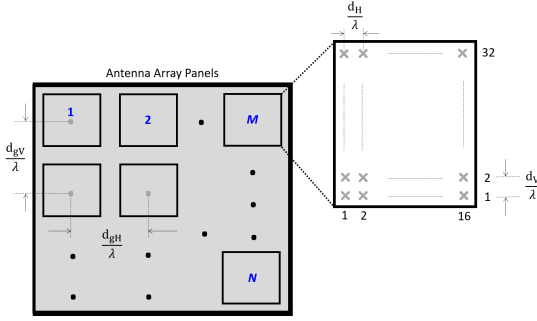


Fig. 1. Cross polarized antenna array panel [62].

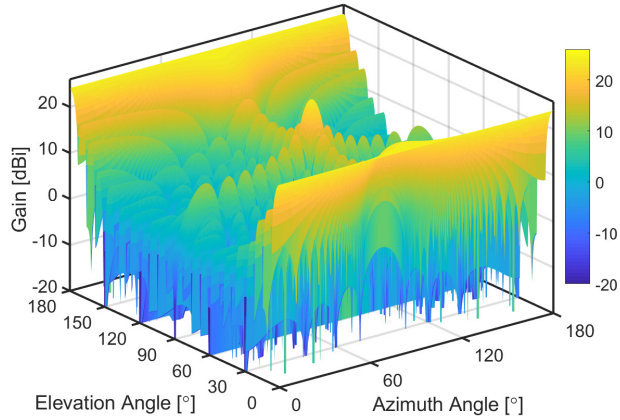


Fig. 2. BS array pattern as a function of azimuth and elevation scan angles [68].

antenna modeling [62], [63]. Figs. 2 and 3 show the BS and UE array radiation pattern based on parameters as defined in [62, Table 7.3-1, page 22].

D. Summary

The mmWave channel when considered for indoor applications differs from the microwave channel in key aspects such as free space path loss, diffraction, and penetration loss with respect to different surfaces. This required the need for different measurements to be done for channel characterization. Some key results are presented in Section II-B. Path loss equations and penetration loss for indoor scenarios can be found in [62, Tables 7.4.1-1 and 7.4.3-1]. Various channel models have been developed, these include those by 3GPP [62], ITU-R [63], METIS [57], MiWEBA [69], Fraunhofer HHI's QuaDRiGa [65], COST2100 [70], NYUSIM [71] which still has ongoing measurements for indoor scenarios. The channel models are all GSCM-based with added cluster based modeling. Small-scale parameter values are further available when considering indoor scenarios found in the documentations mentioned for corresponding models.

Several measurements have been done in the mmWave band for outdoor (urban macro and urban micro) scenarios but the indoor measurements are limited to the sub-6 Ghz band for the channel models developed with the exception of [72], where the authors propose an extension for an indoor channel model based on extensive measurements

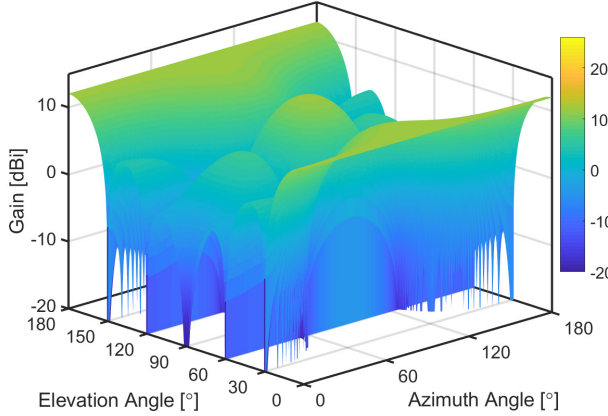


Fig. 3. UE array pattern as a function of azimuth and elevation scan angles [68].

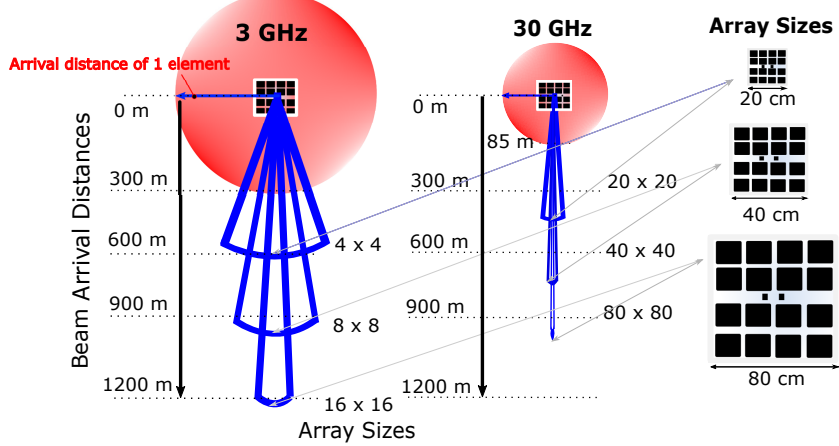


Fig. 4. Effect of beamwidth relative to operating frequency and array sizes [28].

carried out at 28 and 140 GHz. We observe that indoor channel models are an extension of outdoor ones, and can be adapted easily based on the delay and angular spreads of any environment, as well as by adapting path loss modeling.

III. IMPLICATIONS OF BEAMFORMING ARCHITECTURES FOR MMWAVE LOCALIZATION

It is a common misconception that for higher frequencies the free space propagation loss is higher. As explained in [73], for given aperture area of the antennas used, shorter wavelengths propagate farther due to the narrow directive beams. This is further verified in [74] with a patch antenna operated at 3 GHz and an antenna array operated at 30 GHz of the same physical size. We see equal amount of propagation loss irrespective of the operating frequency. Thus, mmWave frequencies enable the use of antenna arrays that produce highly directional beams which lead to large array gains. This can be observed from Fig. 4, which shows not only the increase in array size with respect to the beam penetration distance, but also how the larger array size increases the coverage area [28].

A. Analog beamforming

Analog beamforming, sometimes also referred to as beam steering, is done by connecting a single RF chain to a string of phase shifters that are both energy- and cost- efficient. Each phase shifter multiplies its input by $e^{\frac{j2\pi}{2^N}}$, where $j = \sqrt{-1}$, N is the number of bits, and $k = 0, \dots, 2N - 1$ is used to control the phase shifters. Most commonly, codebook-based schemes are used to steer the beams in the direction of the UE/receiver. At the receiver, the received signal strength indicator (RSSI) is the most commonly used parameter to estimate the direction of arrival and delay, and thus localize the device. However, phase shifters have a constant amplitude constraint and limited phase resolution. It is also worth noting that analog beamforming converges to a single beam for multiple data transmissions, and in multi-user case the inter-user interference is very high. This is a drawback for localization applications, as the phase resolution for analog beamforming is low. The popularity of analog beamforming systems comes from the availability of commercial off-the-shelf (COTS) devices, that are being used for research on mmWave positioning. The devices come with a pre-programmed codebook to generate beam patterns and with support for retrieving the RSSI and channel state information (CSI) which can be used to isolate the position of the UE. We discuss the hardware devices used in more detail in Section V-C.

B. Hybrid beamforming

Hybrid beamforming is by far the most researched form of beamforming. It gives a middle ground between complexity and cost. Here, the analog beamformer is used in the RF domain, along with a digital precoder at baseband. This can be either a fully connected structure or a partially connected one. Hybrid analog/digital beamforming structures provide balance between the beam resolution and cost and power consumption. By using multiple RF chains concurrently, beam sweeping can be done in a short time leading to shorter beam training time which leads to higher effective data rate. At mmWave frequencies the sparse channel behaviour is useful for beam training and higher array gains. Multiple hybrid beamforming techniques for mmWave have been proposed in the last ten years which broadly fall under codebook dependent, spatially sparse precoding, antenna selection and beam selection [75]. [76] first gave the idea of what we call hybrid beamforming today. It was a combination of a digital baseband precoder and an RF precoder which falls under spatially sparse precoding. The work in [77] first proposed the idea of baseband beamforming, or “hybrid beamforming” as the authors named it, that chooses the best RF beam based on a capacity maximization criterion, and then derives a zero-forcing (ZF)-based weighing matrix for digital precoding. Also, both [78] and [79] suggest codebook-based precoding solutions. Recent works have proposed compressive sensing, least squares- and discrete Fourier transform (DFT)-based solutions for hybrid beamforming with use cases in car-to-car scenarios and high speed trains. In most cases, hybrid beamforming is seen to perform as well as fully-digital beamforming, and as being both cost-effective and spectrally efficient.

C. Digital beamforming

Digital beamforming adjusts the amplitude and phase of the transmitted signals using precoding. Linear precoding algorithms such as matched filter (MF), ZF, and regularized zero-forcing (RZF) methods were classically used for single-antenna user systems. For multiple-antenna users, block diagonalization is a feasible approach. Digital

beamforming can be considered as paradise for mmWave positioning. With the possibility of huge antenna arrays (256×128 upwards) a beam resolution of the order of centimeters can be achieved. The calibration accuracy of digital systems allows us to use high-resolution parameter estimation algorithms that can estimate not only the time of arrival (ToA) and AoA but also the Doppler frequency offset in case of mobility, making it possible to update the position of a UE in real-time. The issue here arises from the use of a RF chain per antenna, which leads to a complex, non-cost-effective hardware system for massive multiple-input multiple-output (MIMO) structures.

As digital beamforming offers higher beam resolution, it is a viable candidate where multi user mmWave or rather mmWave massive MIMO systems are considered. However, commercial hardware for a fully digital system is still in its infancy, and only laboratory results exist. Several authors have proposed alternative techniques for the realization of a digital system that is power efficient. For instance [80] gives an option for digital beamforming that employs switches to bypass the hardware constraint of using multiple RF chains. In [81]–[83], the authors propose different ways to form an antenna array using waveguides and printed circuit boards that support digital beamforming. Alternatively, [80], [84] propose novel frameworks to do digital beamforming for a mmWave setup using linearization to help with power amplifier loss and improved quantization.

D. Performance vs. complexity overview

In localization applications, the requirement for mmWave indoor systems is to isolate the position of the receiver inside a room, while taking into account blockage caused by humans and objects alike, with LoS being the dominant multipath component. The presence of pillars, metal and glass surfaces affects the channel impulse response and thus make it difficult to extract position information. Presence of antenna arrays greatly enhances the accuracy of the position coordinates. Whereas digital systems have cleaner isolated beams and can potentially yield centimeter-level pointing accuracy, analog setups have a limit to the number of beam patterns they can generate: when trying to increase the resolution, these beam patterns eventually start to overlap. As stated above, the number of *beams* is proportional to the number of available RF chains, thus increasing the complexity hundred-fold for digital systems. Calibration issues also prevent analog systems from performing high-resolution parameter estimation which could improve the localization accuracy. Hybrid beamforming seems a promising tradeoff as of now, due to the easier availability of COTS devices, and to a performance almost as good as that of fully digital systems.

IV. PROGRESS IN STANDARDIZATION OF CELLULAR MMWAVE SYSTEMS

From a communications perspective, the standardization of fifth-generation (5G) systems by the 3GPP Release 15-17 has involved multiple frequency bands. Namely, the existing bands below 7.25 GHz (FR-I region) act as a key workhorse of 5G systems, while bands between 7.25 GHz and 71 GHz (FR-II region), some of which fall in the mmWave regime, are also heavily relied upon. These bands were proposed by the ITU-R at the 2015 World Radio Conference (WRC), and approved at ITU-R WRC 2019. In addition to the FR-I bands, the following FR-II bands were approved (in GHz): 24.25–27.5; 31.8–43.5; 45.5–50.2; 50.4–52.6; 66–71. The FR-II bands enable a significant increase in available bandwidths relative to FR-I, and are managed via licensed access mechanisms such as enhanced UTRA-dual connectivity (EN-DC). Furthermore, existing satellite and fixed wireless services in some of

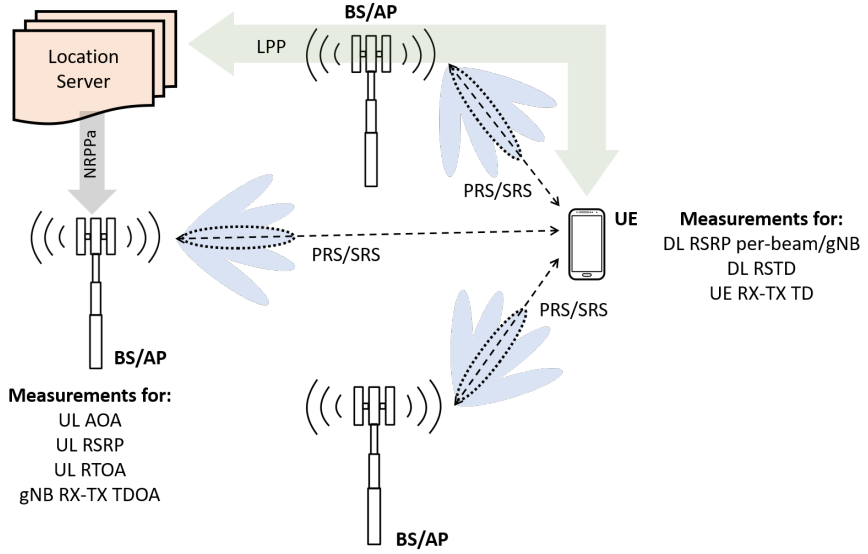


Fig. 5. 3GPP Release 16 radio access type-dependent architecture standardized for UE localization in URLLC scenarios. All BSs/APs are interfaced with a centralized unit enroute to a URLLC core network.

the above bands need to co-exist and be managed along with terrestrial access, fronthaul and backhaul, respectively. From early commercial deployments, it is observed that licensed approaches amongst multiple operators result in spectrum congestion, so that novel forms of spectrum access/coordination mechanisms are implemented.¹

In 3GPP Release 16, localization of UEs has served as a major study item in the context of URLLC use case. For many years, UE localization has been accomplished with Global Navigation Satellite Systems assisted by cellular networks. This approach has been known to provide accurate localization, yet it is typically limited to outdoor areas with high-level of satellite visibility. However, there is currently a range of applications that require accurate localization not only outdoors, but also for indoor environments. Architecture-wise, localization in 5G is based on the use of a location server, similar to long-term evolution-advanced (LTE-A) systems. The location server collects and distributes information related to localization (UE capabilities, assistance data, measurements, position estimates, etc.) to the other entities involved in the localization procedures. A range of localization methods based on downlink or uplink communications, are used separately or in combination to meet accuracy requirements for different scenarios.

Downlink-based localization is supported by providing a new reference signal called the positioning reference signal (PRS). Compared to LTE-Advanced, the PRS has a more regular structure and a much larger bandwidth, which allows for a more precise correlation and ToA estimation. The UE can then report the ToA difference for PRSs received from multiple distinct BSs/APs, and the location server can use the reports to determine the position of the UE.

Uplink-based localization is based on the canonical 3GPP Release 15 sounding reference signals (SRSs) with

¹We note that these are operator and vendor specific, since band combinations vary depending on the specific country.

Release 16 extensions. Based on the received SRSs, the BSs/APs can measure and report (to the location server) the arrival time, the received power and the AoAs from which the position of the UE is estimated. The time difference between downlink reception and uplink transmission can also be reported, and used in round-trip time (RTT) based positioning mechanisms, where the distance between a BS/AP and a UE can be determined based on the estimated RTT. By combining several such RTT measurements, involving different BSs/AP anchors, it becomes possible to estimate the location of the UE. The overall architecture is as depicted in Fig. 5.

We note that these methods do not utilize the full-dimensional nature of the propagation channel (azimuth and elevation domains), and do not fully take into account the phase information needed to estimate the underlying MPCs with high resolution. While this is an ongoing topic for research in many study items of 3GPP Releases 17 and 18, we refer the reader to [85] for further details. Along this same line, a steady stream of work is also conducted in academia, see e.g., [86].

V. DEVICE-BASED MMWAVE LOCALIZATION ALGORITHMS FOR INDOOR COMMUNICATION SYSTEMS

A. Introduction

In this section, we introduce algorithms and methods that leverage lab-grade and commercial-grade mmWave hardware to localize devices indoors. As for any wireless localization process, mmWave devices need to collect some location-dependent measurements (or features) in order to estimate the location of a transmitter or receiver. Like other wireless equipment, mmWave hardware typically outputs baseline measurements such as RSSI and signal-to-noise ratio (SNR), and can collect time of flight (ToF) measurements, through the interaction between the client and an AP.

As remarked in Section III, however, mmWave devices have peculiar characteristics that differentiate them from commonplace WiFi equipment. Specifically, mmWave arrays can incorporate a large number of antennas. The presence of large arrays enable mmWave devices to output low-level physical layer measurements from each antenna separately. Once the device has locked onto a signal, each antenna receives the same signal with a different phase, corresponding to the delay incurred by the signal due to its spatial position in the array. These measurements can be made available as CSI and localization algorithms can exploit them to localize a device, either by converting them into AoA estimates (e.g., [87], [88]) or by directly inferring the location of a device by exploiting the CSI as a location-dependent feature.

Whenever CSI measurements are not available, a device can still retrieve angle information by post-processing the output of standard-compliant beam training procedures. Typically, each mmWave has a number of pre-programmed beam patterns that provide it with the necessary flexibility to focus energy towards different directions. Each beam pattern ideally covers a well-defined portion of the 3D space, so that observing each beam pattern separately makes it possible to implement a scan of all azimuthal and elevation angles that the mmWave array can cover. Therefore, measuring the power received through each beam pattern configuration would implement a sweep of lookout angles. By identifying the beam pattern that leads to the largest received power, a mmWave device could easily identify angles of arrival. We now proceed to discuss each type of location-dependent feature separately in the context of mmWave communications, highlighting the pros and cons of each feature.

B. Pros and cons of location-dependent measurements for mmWave localization

Angles of arrival and departure, angle difference-of-arrival — The term angle of arrival (AoA) refers to the angle at which radio signals illuminate the antenna array at the receiver. The transmitter-based counterpart, the AoD, refers to the angle at which the radio signals emanate from the antenna array at the transmitter front-end in order to reach the receiver. In most cases, more than one antenna elements are required to compute angle information. Other methods to extract AoA information from the receiver array involve the use of CSI, beamforming methods, or subspace approaches such as the well-known multiple signal classification (MUSIC) [89], and estimation of signal parameters via rotational invariance techniques (ESPRIT) [90]. We cover angle-based approaches in Section V-D.

Pros: Relatively accessible information in mmWave systems thanks to the large number of antennas in transmitter and receiver arrays.

Cons: If not associated to some range information, can only yield location estimates in a relative coordinate system. Multipath propagation can distort angle estimates, if not properly modeled or compensated for.

Channel state information (CSI) — CSI refers to measurable properties of a received mmWave signal that relate to the propagation channel linking two devices, e.g., the AP and the client. Different mmWave hardware may provide different forms of CSI. For example, patching TP-Link's Talon routers [91] with special firmware makes it possible to extract receiver-side CSI in the form of one complex gain coefficient per receiving antenna, expressing the attenuation and phase shift that affect the strongest propagation path at each antenna. Post-processing CSI yields different signal parameters, including path attenuation and angle information. If CSI values are sufficiently precise (e.g., no coarse quantization affects the amplitude or phase), collecting receiver-side CSI from multiple antennas also enables the estimation of AoAs. We cover CSI-based approaches in Section V-E.

Pros: Rich information that can be readily used for ranging or as an input to learning-based approaches.

Cons: Typically not available straightforwardly on all devices. Different devices may provide different types of CSI.

RSSI — RSSI is one of the simplest proxies for the range of a device in an environment. It is measured at a receiving device as the power or amplitude of the received RF signal. mmWave received signal strength (RSS) measurements can be extracted from the physical or medium access control (MAC) layer of a device and used to measure the distance of a client from the AP, based on the knowledge of a path loss model. The client is believed to lie on the circumference of the circle centered on the AP and having the estimated range as the radius. Such estimates from more than two APs can be trilaterated to approximate the location of the client. We cover RSSI-based approaches in Section V-F.

Pros: simple ranging method, typically available on communication devices.

Cons: Error prone, typically requires an extensive tuning of the path loss model. RSS measurements are often affected by the losses in the front-end receiver architecture of the client and the number of quantization bits in its ADC circuitry.

Time information — Time information is another common proxy for the distance between two devices. Typical measurements used for this purpose involve ToF and time difference-of-arrival (TDoA) measurements. ToF (also known as ToA) measurements exploit the time taken for a signal to propagate from the AP to the client in order to estimate the distance between them. The client intuitively lies on the circumference of the circle with the AP as the center and the distance estimate as the radius. Multilateration methods can be used to estimate the location of the client. It is important to note that ToF measurements require a tight synchronization between the AP and the client. mmWave signals offer better ToF estimation accuracy (thus better ranging resolution), owing to the large bandwidth available, especially in the unlicensed bands. We cover time-based approaches in Section V-F.

Pros: ToF information is usually accurate when directly extracted from a device’s physical layer, which helps accurate localization. Such protocols as the fine time measurement (FTM) protocol, when available on a device, can provide very accurate timing estimates.

Cons: Requires sub-nanosecond sampling times in a device’s ADC in order to yield a sufficiently fine range resolution.

Hybrid approaches — Several solutions propose to fuse information from multiple sources in order to improve localization accuracy. For example, several works merge AoA and RSSI, or AoA and ToF estimates. We cover hybrid approaches in Section V-G.

Pros: Hybrid schemes usually achieve better accuracy. In some purely angle-based algorithms, side information such as RSSI and ToA can help resolve geometric translation, rotation, and scaling ambiguities.

Cons: The algorithm becomes more complex, and relies on the estimation of multiple quantities. In ill cases, errors compound and make the location system even more inaccurate.

According to our survey of the literature on mmWave localization algorithms and to the above discussion, we identify two broad categories in the available literature:

- 1) Algorithms *tailored* to mmWave communication protocols and schemes, that exploit protocol operations to extract geometric scenario information and infer the location of the devices.
- 2) *General* algorithms that apply well-known range-based or range-free localization approaches to mmWave communications.

Algorithms in the first category are mainly angle-based or CSI-based: they infer the angle of arrival structure by leveraging, e.g., sector measurements in communication protocols. Then, they use angle information to localize a device. By way of contrast, the algorithms in the second category are not necessarily mmWave-specific. These works can be further subdivided by considering where the algorithm mainly runs:

- 1) In *client-centric* algorithms, the intelligence mainly resides on the client, which may collect location-dependent measurements by receiving signals from one or multiple APs, and by estimating its own location locally. This approach is useful for systems that need to scale to up a large number of devices, as each device runs the algorithm independently.

- 2) In *AP-centric* algorithm, the intelligence resides in a computing entity connected to one or multiple APs, which coalesce their measurements from multiple clients in order to estimate the location of each client. These schemes are ideal for seamless network management purposes (e.g., to optimize client-AP associations) but scale less than client-centric approaches when the number of clients increases.
- 3) Schemes based on *AP-client cooperation* are based on a shared intelligence, where both one or more APs and the client run portions of the localization algorithm, and possibly exchange information to finally estimate the client location.

In our scan of the literature, we observed a comparatively small number of works that employ a form of machine learning to compute location estimates. We believe this is due to localization being a somewhat understood problem, whereby the community prefers the use of understandable and optimizable signal processing algorithm rather than training black-box machine learning models. Yet, these prove a feasible solution in some cases, e.g., when a huge database of different location-dependent features is available, and the complexity of the considered indoor environment prevents straightforward modeling.

Table II summarizes the above preliminary subdivision pictorially, in a way that conveys in what category most of the research efforts has concentrated so far. We observe that while a few approaches have considered baseline RSSI, SNR and time measurements to localize mmWave devices, most of the research moved to exploit the fine angle resolution that large or massive mmWave communication arrays enable. A significant number of works also consider hybrid approaches, in an attempt to mix good angle resolution with the extra information yielded by time- or RSSI-based measurements, and thus achieve greater accuracy. Finally, we observe that a few recent works (from 2017 to the time of writing) rely on machine learning techniques, typically to process RSSI and SNR measurements and predict the location of a device. We highlight these works in green in Table II, in order to emphasize the emergence of this previously unobserved paradigm in indoor mmWave localization.

TABLE II
VISUAL REPRESENTATION OF THE CONCENTRATION OF RESEARCH EFFORTS FOR DEVICE-BASED MMWAVE LOCALIZATION.
GREEN ICONS REPRESENT RECENT PAPERS THAT EMPLOY SOME FORM OF MACHINE LEARNING IN THEIR APPROACH.

Indoor mmWave localization					
	Traditional methods		Tailored methods		
	RSSI and SNR	Time information	Angle information	CSI-based	Hybrid approaches
Client-centric					
AP-centric					
AP-client cooperation					

C. mmWave hardware for localization

Localization experiments so far have been carried out using either laboratory-grade or commercial-grade equipment. Laboratory-grade equipment typically includes a software-defined radio (SDR) for signal generation and a mmWave up-converter, with a directional antenna to drive signal emission. For example, the above setup is used in [92], where the authors employ horn antennas to emulate narrow beam patterns. A similar setup has been observed in [93] and [94], where the authors have used the Zynq 7045-based SDR and the universal software radio peripheral (USRP) X310-based SDR respectively, plus a 60-GHz analog front-end to emit the mmWave signals. The authors of [95], [96] have used an NI 60-GHz transceiver SDR systems that allow full programmability of the physical layer (PHY), MAC, and network layer, especially for wireless LAN (WLAN) applications. It also has a 24-element reconfigurable antenna array by Sibeam. A field-programmable gate array (FPGA)-based setup has been discussed in [97], where the authors have used the XCKU040 Kintex UltraScale FPGA for the baseband processing of a 60-GHz reconfigurable phased antenna array architecture. PEM-003 60 GHz transceivers were used as the RF front-end for the experimentation. Recently, a new set of SDR boards, dedicated for the research of mmWave wireless communication, have been developed by a NYU spin-off called Pi-Radio [98]. These Pi-Radio v1 SDRs consist of a 4-channel fully-digital transceiver board with Xilinx's ZCU111 RF system-on-chip (SoC) [99], and operate in the 57-64 GHz frequency band with about 2-GHz bandwidth support.

Alternatively, commercial-grade equipment can be leveraged for localization purposes, usually by flashing the image of custom operating system builds that embed application program interfaces (APIs) to access the output of the beam training procedure. For example, the work in [100] realizes a geometric 3D localization system using a 4×8 phased array within a router that embeds a Qualcomm QCA9006 tri-band chipset for AoA and ToF measurements. The work in [101], instead, taps into the output made available by the Talon AD7200 [91] routers' firmware. In the latter case, the hardware and the interface require significant adaptations of the angle estimation algorithms. For example, the firmware and operating system used in [101] returned coarsely quantized power measurements for each beam pattern and sometimes incomplete measurement outputs, which required to re-cast the angle estimation algorithm to be robust against quantization noise and missing values. The proprietary setup used in [100] returns the raw channel impulse response (CIR) measurements, which are then sanitised to extract the azimuth and elevation angles of arrival from the LoS paths, and the ToF information for distance estimation.

Other works such as [114] also employ COTS devices like the 802.11ad-enabled Airfide AP [115] to enhance the antenna array performance for omni-directional coverage and to improve link resilience in mobile and dynamic environments. Table V-C summarizes the above discussion by relating the works in our survey with the hardware platforms used to validate mmWave localization algorithms. We observe that software-defined platforms are still preferred, due to their greater versatility and to the availability of multiple digital receiver chains. COTS hardware is starting to appear in experimental evaluations, although this typically requires system management skills to flash such hardware with operating system distributions that give access to information from the radio reception chain.

From a practical standpoint, the manufacturers of commercial-grade mmWave devices typically define a code-book of antenna weights that drive beam patterns to cover the largest set of lookout directions. As a result, the

TABLE III
SUMMARY OF THE HARDWARE PLATFORMS USED IN MMWAVE LOCALIZATION ALGORITHMS

Hardware Platform	Related Literature
Vubiq 60 GHz Development system	[92], [101], [102], [103]
Zynq 7045 based SDR with 60 GHz analog front-end	[94]
4×8 phased array AP with QCA9006 triband chipset	[100]
TP-Link Talon AD7200	[104], [105], [106], [107], [108], [109]
QCA6320 baseband module with QCA6310 RF front-end	[110]
NYURay 3-D mmWave ray tracer	[111]
USRP X310 and TwinRX daughterboard with 60 GHz analog front-end	[112]
MicroTik wAP 60G	[113]

corresponding beam patterns are not necessarily narrow, nor do they necessarily present a single direction where the gain is maximum [116].

Yet, standard-compliant beam training procedures still help retrieve location-dependent measurements through an automated process that is typically natively implemented in every device. For example, the 802.11ad standard [15] presents a two-phase beam training process:

- *Sector-level sweep (SLS)*: During this phase, the transmitter (or *beamformer*) periodically transmits sector sweep (SSW) frames using the different beam patterns defined in the sector codebook. The receiver (or *beamformee*), receives these frames omnidirectionally and sends back an acknowledgment with the transmit sector yielding the highest signal quality. Subsequently, the two devices swap roles, and the receiver selects its best transmit sector. This phase provides coarse-grained beam patterns that are best suited for the two communicating devices.
- *Beam refinement protocol (BRP)*: This optional phase can be used to refine the beam patterns chosen after the SLS phase. The BRP process is iterative. The two devices exchange special BRP packets requesting and acknowledging the transmit (TX) and receive (RX) training requests (TX-TRN and RX-TRN). The result is fine-grained beam patterns for the transmission and reception of the data, resulting in not just better directivity and therefore higher-throughput links, but also in a higher correlation between the beam pattern used and the AoA of a signal.

These phases occur during the association beamforming training (A-BFT) subinterval of the beacon interval (BI), as part of the channel access mechanism. The beamforming process during the data transmission interval (DTI) is to handle device mobility, blockage, etc. The BI frame for channel access is shown in Fig. 6 and the two beamforming phases are illustrated in Fig. 7.

The more recent 802.11ay standard [117] formalized beam training procedures that enhance those of 802.11ad, namely the beam refinement protocol transmit sweep (BRP TXSS) and the asymmetric beamforming training (ABT) procedures [17]. These procedures rely on a channel reciprocity assumption both to speed up beam training (through the *BRP TXSS* scheme) and by slightly modifying the process to compensate for the possibly different antenna gains at the AP and at the client. In addition 802.11ay speeds up training in the presence of several clients through group beamforming, which enables beam training with multiple clients simultaneously.

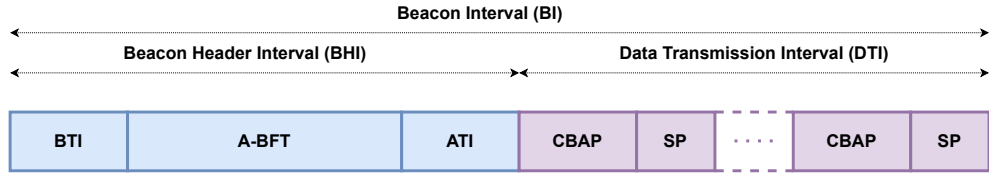


Fig. 6. Beacon Interval frame of the IEEE 802.11ad standard [15]. It is important to note that after beam training process, STAs contend for the channel during the contention based access period (CBAP) and access it contention-free during the service period (SP).

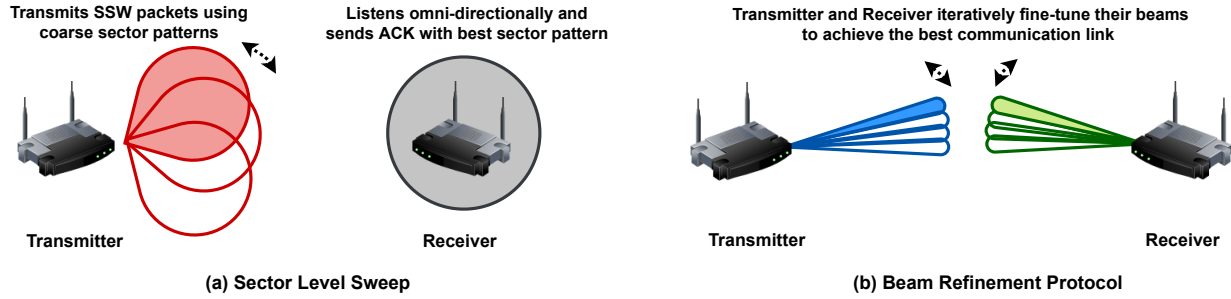


Fig. 7. A simple illustration of the sector level sweep and beam refinement protocol as proposed in the IEEE 802.11ad standard [15].

When run with generic beam patterns, the above procedures do not trace a one-to-one relationship between the angle of arrival or departure of a mmWave signal and the antenna configuration that leads to the highest received power. Yet, if the beam patterns of the codebook are known, a mmWave device can still estimate angles of arrival via signal processing techniques involving compressive sensing [116], or linear programming and Fourier analysis [101]. Knowing angles of arrival enables angle-based localization techniques, with the additional advantage that angle estimation hinges on standard beam training procedures, with no need for external hardware components. In other words, localization becomes an embedded feature of mmWave communications. In the following subsections, we explain the details of each surveyed work, and provide a synopsis of the main results of each paper, the main enabling techniques, and the performance evaluation methods employed in the form of summary tables at the end of the section.

D. Angle-based algorithms

AoA measurements, alongside the quasi-optical nature of mmWave signal propagation, facilitate high-accuracy localization based on triangulation. This is the simplest approach to localization using AoA, wherein the angle information from the transmitting APs and simple geometric principles are used to compute the client's position. In a 2-D plane, such position can be estimated using just two APs [118].

Geometric methods are the simplest methods for localization when using AoA estimates. In [102], the authors present three lightweight single-anchor algorithms based on the AoA measurements. These algorithms are based on triangulation, angle difference-of-arrival (ADoA), and fingerprinting, respectively. The algorithms have been

simulated and also experimentally validated on pre-standard mmWave hardware operating at 60 GHz, showing that they achieve sub-meter accuracy with high probability, given the AoA estimate errors are low.

The simplicity of these algorithms motivated the authors of [103] to generalize the schemes in [102] for any number of APs. These algorithms are extensively simulated as well as experimentally validated on 60 GHz COTS devices, in different indoor scenarios against two benchmark algorithms based on fingerprinting and AoA. The two algorithms provide sub-meter accuracy in most indoor environments with multiple antennas. Triangulation-based scheme performs slightly better than the ADoA-based one in most scenarios, but independence of orientation and compass bias makes ADoA more preferable.

The ideas proposed by [102] have also been used by the authors of [119] for context inference and obstacle detection. They use the TV and ADoA algorithms for receiver localization using one AP, estimate the locations of virtual anchor nodes, and thus infer the presence of obstacles.

AoA measurements have also been used for simultaneous localization and mapping (SLAM). For example, in [120], the authors propose a joint access point and device localization (JADE) algorithm that jointly maps the location of the client and of the physical and virtual APs, while mapping the indoor environment, without any prior information (i.e. number of access points, boundaries of the room, etc.). The algorithm measures AoAs from the beam training procedure and leverages ADoAs to estimate the location of the APs and then of the client. Environment mapping follows by matching physical and virtual anchors and by predicting reflection points on surrounding surfaces. Simulation results show sub-meter accuracy in 90% of the cases, even for erroneous AoA estimates. JADE outperforms the approaches in [103] in almost all scenarios.

A similar algorithm that exploits AoA information to derive ADoA estimates and fuses multiple measurements at different locations is CLAM [92]. Like in [120], the algorithm proceeds by first estimating the location of the anchor APs, then of the client, and finally of the environment's boundaries. The algorithm is simulated and experimentally evaluated, showing sub-meter device localization errors in about 90% of the cases.

In [121], the authors present mobile device positioning scheme in an indoor mmWave massive multiple-input single-output (MISO) scenario. The two-fold scheme utilizes coarse-grained AoD information from mobile clients with a single antenna to estimate the position of each client via downlink transmissions using adaptive beamforming.

E. CSI-based algorithms

In recent works, mmWave channel estimation techniques have also been used to estimate the location of the client. One such work is presented in [122], where the authors present a channel parameter estimation method that transforms the mmWave uplink training signal into a higher-dimensional tensor using the canonical polyadic model. Tensor factorization using the proposed generalized structured canonical polyadic decomposition results in time delay, AoA, and path fading coefficient estimates. These parameters are used to estimate the locations of the mobile device.

A different way to exploit uplink CSI estimates [104] requires that the APs convert the LoS CSI measurements into angle information and then localize the client. The system is implemented on Talon AD7200 router (without

interfering with 802.11ad operations), and the authors propose to employ the location estimates to optimize AP-client associations. The proposed system achieves sub-meter localization accuracy in about 80% of the cases.

With a focus on localizing passive objects, in [123] the authors use the CIR captured after reflection from different objects and surfaces in an indoor environment to detect objects and also model the indoor environment in 2D. The proposed method has been evaluated using a testbed developed specifically for this purpose.

F. RSSI and ToF

RSSI and SNR based localization systems generally employ trilateration or fingerprinting-based techniques to localize the client. A number of works in the literature illustrate this concept. The authors in [124] investigate trilateration-based localization algorithm using RSSI measurements for 60-GHz IEEE 802.11ad WLANs. They modify the trilateration algorithm based on the concept of (weighted) center of mass. Simulations on randomly generated data points and the RSSI measured based on the IEEE 802.11ad channel model result in an average positioning error of about 1 m. This is among the earliest works on mmWave-based indoor localization that leverages RSSI measurements.

RSSI is also the foundation of several fingerprinting-based localization schemes, especially in sub-6 GHz wireless networks. The authors of [105] propose a localization system that generates fingerprints of transmit beam indices and the corresponding RSS measurements between a pair of mmWave devices. Probabilistic location models are generated based on the fingerprint data and are leveraged for location estimation. The algorithm is experimentally evaluated using 60 GHz COTS devices. Many times, SNR-based fingerprinting is also at the core of some mmWave localization works, especially in combination with machine learning and deep learning techniques. The authors of [106] propose machine learning regression models for localization in warehouses. SNR information is collected from Talon AD7200 routers. The supervised regression models are trained offline and then deployed for localization at run time. The proposed method achieves sub-meter accuracy in 90% of the cases.

Similar machine learning regression models have been used for location estimation in [107], where the authors use spatial beam SNR values, typically available during the beam training phase, in order to generate a location- and orientation-dependent fingerprint database. Deep learning techniques are also the main enablers for localization in [108] and [109], where the authors proposed ResNet-inspired models [125] for device localization in LoS and NLoS scenarios. To tackle the challenges imposed by NLoS conditions, the authors use spatial beam SNR values in [108], whereas they employ multi-channel beam covariance matrix images in [109].

One example of how ToF measurements have been used in the mmWave context is presented in [94]. Here, the authors present a two-way ranging based on round-trip ToF (RTToF) information. The scheme estimates the distance between master and slave nodes, and then trilaterates the position of the slaves. The authors implement their algorithm on an SDR with a 60 GHz SoC. The proposed system achieves an average distance estimation of 3 cm and an average positioning error below 5 cm.

G. Hybrid approaches

A combination of two or more techniques mentioned above can be used to build systems that achieve better localization or mapping accuracy, with respect to stand-alone techniques. Coupling different sources of information is useful in challenging environments, where some mmWave parameter measurements may fail.

Angle information along with RSSI-based ranging are the foundation of several mmWave localization approaches in the literature. The authors in [126] propose a positioning algorithm using RSS and AoA measurements. These measurements are derived from a channel compression scheme designed for a mmWave mMIMO scenario with only one AP. The RSS and AoA estimates from the above methods are employed for position estimation. The system provides decimeter-level accuracy even at low SNR, and even lower errors as the SNR increases.

As opposed to ranging, the algorithms proposed in [127] and [128] are based on location fingerprinting. In particular, the authors measure RSSI and AoA information at various reference points in an indoor environment to generate location fingerprints. K fingerprints nearest to the client measurement are selected from the dataset, and the location estimate corresponds to the weighted average of these K reference points. The algorithm has been simulated with 2.4 GHz and 60 GHz, showing that the average position error is much lower for mmWave signals than lower-frequency signals. To solve the problem of collecting a sufficiently large dataset, [128] generates 3D beam fingerprints using RSSI and beam information. Weighted K-NN was used to localize an unmanned aerial vehicle (UAV) in GPS-denied indoor environments. Particle filters were used along with the imperfect location estimates to track the motion UAVs. The proposed scheme was experimentally validated, and the results showed sub-meter positioning accuracy on average.

RSS jointly with AoA information enables *mmRanger* [110] to autonomously map an indoor environment without infrastructure support. The *mmRanger* scheme senses the environment and uses time domain RSS sequences to reconstruct the path geometry via a path disentanglement algorithm. Then, AoA and RSS information from the reflecting surfaces are exploited to reconstruct the geometries of each surface. Moreover, a robot pedometer assembles all estimated fragments to form a complete map of the environment. The results of the proposed system implementation show a mean estimation error of 16 cm for reflection points, and a maximum error of 1.72 m.

In [101], the authors leverage coarse-grained per-beam pattern SNR measurements provided by a modified operating system flashed on multiple TP-Link Talon AD7200 802.11ad-compliant COTS mmWave router. The AoA estimation problem is formulated using linear programming, and the location is estimated using a modified particle filter and a Fourier analysis-based goodness function. The proposed scheme is experimentally validated and the system achieves sub-meter accuracy in 70% of the cases. AoD and SNR information were used in [129] to design beam-based midline intersection and beam scaling-based positioning algorithms. These were evaluated using both ray-tracing simulation and a WiGig SoC transceiver. The experiments, carried out under LoS conditions, yielded centimeter-level location estimation errors.

Time-based measurements are often enriched with angle information in order to achieve better positioning accuracy, especially for mmWave systems. For example, in [100], the authors propose *mWaveLoc*. The proposed system uses measured CIRs to calculate AoA and ToF data. The system is implemented on IEEE 802.11ad off-

the-shelf devices leveraging the OpenWRT operating system, and achieves centimeter-level distance estimation and decimeter level 3D localization accuracy (median error 75 cm and sub-meter error in 73% of the cases) in a realistic indoor environment. The system has also been evaluated in various experimental conditions.

The author of [111] propose a map-assisted positioning technique using the fusion of ToF and AoD/AoA information. A 3D map of the environment is either generated on the fly or assumed to be known a-priori. The scheme measures a set of possible user locations by fusing the estimated ToF values with angle information. These estimated locations are clustered, and the cluster centroid is output the final location estimate. The algorithm is simulated on the data collected at 28 GHz and 73 GHz by a 3D ray tracer. The best-case and the worst-case mean localization error is found to be about 12 cm and 39 cm respectively.

Instead of explicitly fusing ToF and AoA information, the authors of [130] propose a pseudo-lateration protocol, that enacts the three following steps: i) sector sweeping for tracking LoS and NLoS paths to compute physical and virtual anchors, respectively; ii) angular offsets measurements using extended sector sweeping; and iii) ToF measurements for distance estimation. A post-processing stage is employed for position estimation. The protocol has been simulated and implemented using a 60 GHz mmWave testbed. The protocol implementation achieves centimeter-level location estimation accuracy within 1.5 m and decimeter accuracy beyond 1.5 m.

The authors of [131] explored adaptive filters for motion-assisted indoor positioning. An improved LMS filter estimates the AoA of the client by using the client location, velocity and measured ToF as the inputs. AoA and ToA estimates are fed to an unscented Kalman filter (UKF) to track the client's position. The two-stage algorithm is simulated in an office environment with one AP and achieves centimeter-level positioning accuracy.

Because mistaking LoS for NLoS paths may offset location estimates significantly, the authors of [132] propose a scheme to tell apart mmWave LoS and NLoS MPCs having incurred up to one reflection. For this, they use TDoA and AoA information and apply the mean shift clustering technique. Then, they apply an AoA-based localization scheme that computes least-squares estimates. The methods show a 98.87% accuracy in path identification and positioning error of less than 75 cm in 90% of the cases. NLoS scenarios have also been exploited in [133], where the authors propose a positioning scheme that relies on differential angle information, which is independent of angular reference. This scheme has been evaluated in an indoor environment with a geometric ray tracer based on an IEEE 802.11ay channel model, and achieves sub-30 cm position estimation errors in 90% of the cases.

In [134], the authors present schemes for localization, mapping, obstacle detection and classification. Localization and mapping make use of AoA and ToA measurements to estimate the location of the receiver and of virtual anchors. The latter are used to detect obstacles by estimating reflection points. Snell's law and the relationship between the RSS and the reflection coefficient are used to classify the obstacles based on material composition. The presented algorithms have been simulated in an indoor environment.

Besides locating a client, the schemes presented in [134] have been integrated into a SLAM framework in [135]. This framework involves algorithms for localization, obstacle mapping and tracking. Extended Kalman filter (EKF)-based tracking helps improve obstacle detection and mapping. The framework has been simulated in an indoor environment, yielding sub-meter errors in 90% of the cases. In the same context, the EKF improves the obstacle mapping accuracy to sub-centimeter.

In [112], the authors present a device localization scheme, where the AP and the client are equipped both with sub-6 GHz and with mmWave technology. Sub-6 GHz antennas are used for AoA estimation and mmWave antennas are fed with the AoA estimates for subsequent beam training and two-way ranging. The proposed method has been experimentally validated using SDR platforms, both in an anechoic chamber and in an office environment. Results show 2° AoA errors and centimeter-level ranging accuracy in the anechoic chamber, and 5° AoA error with an average 16-cm range error in the second one.

In [113], the authors propose to track the changes in the CIR measured at the station, that is equipped with an FPGA-based platform with IEEE 802.11ad, in order to localize a device-free object in an indoor industrial environment. The station uses the estimated CIR to measure the AoD and ToF of the signal reflecting off a moving object. Tracking CIR changes over time helps classify the reflections as static or mobile. Then, a Kalman filter smooths the trajectory of the mobile object. The results show sub-meter location errors in all scenarios, and a mean accuracy of 6.5 cm.

H. Summary

We summarize the findings of our survey in Table IV. The table succinctly conveys the main proposition of each paper, the main techniques used among those outlined in Sections V-D to V-G, the tools employed, and a highlight of the performance attained. We observe a number of mmWave localization approaches exploiting different features of mmWave signals as well as different properties of mmWave propagation. While some schemes rely on well-known techniques, e.g., based on ToF and RSSI measurements, these techniques leverage the sparsity of mmWave multipath patterns in order to achieve better measurements and fine time resolution. In some environments and with lab-grade hardware, this often yields decimeter- or sub-decimeter-level accuracy, but requires specific protocols to exchange the data required to localize a device.

With respect to such approaches, angle-based localization schemes relying on AoA and ADaA measurements still prove accurate, and yield the additional benefit that AoA measurements are a direct result of beam training operations at link setup time. Hybrid solutions that leverage both angle information and time/RSSI information tend to show even better performance, although but a few of them has been tested in operational environments with COTS equipment.

Table VI supports the above discussion by summarizing the techniques employed in each of the surveyed works. We observe a preference for geometry-based localization approaches, with different supporting signal processing algorithms. Machine learning methods have found comparatively less application to date. A possible explanation of this fact is that training these algorithms requires sufficiently large datasets which are often difficult to obtain. A valuable contribution to the community, in this respect, would be a collaborative effort towards a public benchmark dataset, that different authors would use to feed different machine learning approaches.

Finally, Table VII summarizes the performance evaluation approach taken in each surveyed paper. We observe a majority of evaluation based on experiments with real hardware, although simulation is still used in several contexts, e.g., as a proxy to quickly and affordably generate large datasets.

TABLE IV
SUMMARY OF THE LITERATURE ON INDOOR MMWAVE LOCALIZATION

Proposition	Techniques	Tools Used	Performance
Localization Algorithms			
Round-trip time based localization [94]	ToF	Geometry	Distance estimation error within 3 cm and location estimation error within 5 cm.
Accurate 3D indoor localization using a single AP [100]	AoA-ToF	Geometry	3-D localization with median accuracy of 75 cm with sub-meter accuracy in 73% of the cases.
Improving localization accuracy [101]	AoD, RSSI	Linear programming, Fourier analysis, Particle filters	Sub-meter accuracy in 70% of the cases.
Improving the accuracy of device localization [102], [103]	AoA	Geometry	Sub-meter localization accuracy in 70% of the cases.
Improving location estimation accuracy and network performance [104]	CSI	Regression trees, Extended Kalman filter	Sub-meter localization accuracy in 80% cases and throughput improvement between 8.5% and 57%, lesser outage probability, SNR within 3 dB of optimum.
Fingerprinting based indoor localization [105]	RSSI	Probabilistic models	Mean and median localization error of \approx 30 cm.
Indoor localization for intelligent material handling [106]	SNR	Multi layer perceptron regression, Support vector regression, Logistic regression	Centimeter-level accuracy with root mean square error (RMSE) of 0.84 m and MAE of 0.37 m.
Fingerprinting based indoor localization [107], [108]	SNR	Machine learning algorithms, Deep learning	Avg. RMSE is 17.5 cm with coordinate estimates within 26.9 cm in 95% of the cases. Median and mean RMSE of 9.5 cm and 11.1 cm respectively.
Fingerprinting based indoor localization in NLoS environments [109]	SNR	Deep learning, Machine learning algorithms	Location classification accuracy greater than 80%. Median location estimation error of about 11 cm.
Map-assisted indoor localization [111]	AoA, AoD, ToA	Geometry	Mean localization accuracy of 12.6 cm and 16.3 cm in LoS and NLoS respectively.
Sub-6 GHz-assisted device localization [112]	ToF-AoA	MUSIC, Geometry	AoA estimation error less than 5° and about 16 cm distance estimation error.
Single-antenna client localization using downlink transmissions [121]	AoD	Adaptive beamforming	60% improvement in the accuracy in the downlink scenario as compared to in the uplink scenario.
Indoor positioning for wideband multiuser millimeter wave systems [122]	CSI	Tensor decomposition, Clustering methods	Decimeter-level position estimation errors.
Indoor network localization [124]	RSSI	Geometry	Mean positioning error around 1 m.
3D indoor positioning for mmWave massive MIMO systems [126]	AoA-RSSI	Geometry	Low complexity channel compression and beamspace estimation developed. Decimeter-level positioning errors achieved in NLoS scenarios.
Location fingerprint-based localization [127]	AoA-RSSI	K-nearest neighbours	Average positioning error for mmWave is 4 times less compared to lower frequency signals.
UAV positioning in GPS-denied environments [128]	RSSI	Weighted K-NN, Particle filters	Sub-meter 90th-percentile location errors in different cases.
Beam-based UE positioning in indoor environment [129]	SNR, AoD	Geometry	Centimeter-level estimation error in all cases. Experimental results approach the simulations results with MSE difference of 0.1 m.

Single RF chain-based localization [130]	ToF-AoA	Geometry	Centimeter accuracy in location estimation within 1.5 m and decimeter accuracy beyond 1.5 m.
Motion feature-based 3D indoor positioning [131]	AoA-ToA	least mean squares (LMS) and Kalman filters	Centimeter-level positioning accuracy.
LoS and NLoS path identification and localization [132]	TDOA, AOA	Mean shift clustering, Geometry	98.87% accuracy in path identification and positioning accuracy ≤ 0.753 m in 90% of the cases.
NLoS mmWave indoor positioning [133]	AoA, AoD, ToA	Geometry, Levenberg-Marquardt (LM) method	Positioning accuracy within 30 cm in 90% of the observations with differential angle information along with time information.
5G mmWave indoor positioning [136]	RSSI	Geometry, Beamforming	Single-beam geometric model for indoor positioning. Mean error of 0.7 m for stationary in LoS and 2.4 m for a mobile user in LoS/NLoS scenario.
Data-driven indoor localization [137]	AoA	Multi-layer perceptron, Deep learning	Sub-meter localization accuracy.

Localization and Mapping Algorithms

Autonomous environment mapping [110]	RSSI, AoA	Geometry, K-means clustering	Reflection point mean estimation error of 16 cm with a max error of 1.72 m.
Passive object localization [113]	AoD, ToF	Kalman filters	Sub-meter accuracy in all cases with 6.5 cm mean error accuracy.
Localization and obstacle detection [119]	AoA	Geometry	Sub-meter accuracy in 70% of the cases. High accuracy obstacle detection and obstacle limits estimation.
Localization and mapping [92], [120]	AoA	Geometry	Sub-meter localization accuracy in 90% of the cases. SLAM without any prior knowledge.
Accurate object detection [123]	CIR	Geometry	Accuracy of about 2 cm achieved in most experiments.
Simultaneous localization and mapping without a-priori knowledge [134], [135]	AoA, ToF, RSSI	Geometry, Extended Kalman filters	Sub-meter device localization accuracy in 90% of the cases. Sub-centimeter obstacle mapping accuracy.
3-D localization and mapping [138]	RSSI, AoA, ToA	Geometry	Perfectly maps the environment for AoA errors $\leq 5^\circ$.

TABLE VI
SUMMARY OF THE MAIN TECHNIQUES USED IN THE SURVEYED PAPERS

Analytical Tools	Related Literature
Beamforming techniques	[121]
Clustering methods	[110], [122], [132]
Deep learning	[108], [109], [137]
Fourier analysis	[101]
Geometry	[94], [100], [102], [103], [111], [119], [124], [129], [134], [136], [138]
Kalman filters	[104], [113] [131], [135]
Least mean square filters	[131]
Levenberg-Marquardt (LM) method	[133]
Linear programming	[101]
Machine learning models	[127], [128], [137], [106], [107]
MUSIC	[112]
Particle filters	[101], [128]
Probabilistic data modelling	[105]
Tensor analysis	[122]

TABLE VII
SUMMARY OF THE EVALUATION METHODS USED IN THE MMWAVE LOCALIZATION ALGORITHMS

Evaluation	Related Literature
Experimentation	[92], [94], [100], [101], [102], [103], [123], [105], [106], [107], [108], [109], [110], [111], [112], [113], [128], [129]
Simulation	[119], [121], [122], [124], [126], [127], [130], [131], [132], [133], [134], [135], [136], [138]

VI. MMWAVE RADAR-ENABLED DEVICE-FREE LOCALIZATION AND SENSING

A. Introduction

In this section, we focus on mmWave-based radar systems that operate over short distances (a few tens of meters), which have recently emerged as a low-power and viable technology for environment sensing. These devices are expected to find extensive use in a number of relevant applications, by replacing standard camera-based systems, either fully or in part. Survey papers have been recently published on mmWave sensing, with a focus on signal processing [139] (both with traditional and machine learning-based approaches) and applications [140]. In our review, we emphasize the main signal processing algorithms that are being successfully exploited for indoor sensing, discussing their pros and cons. In doing this, we especially focus on neural network algorithms, discussing their different flavors and the most promising research directions. An illustrative overview of the main techniques used for sensing applications that exploit mmWave radars is provided in Fig. 8.

Two main components of a radar device are TX and RX RF antennas, which are combined with an ADC, micro-controller units (MCUs), digital signal processors (DSPs) and a clock. The main idea behind such a system is to transmit a properly shaped radio wave (e.g., pulses or continuous waves) and estimate the modifications that occur in the back-scattered copy of such wave, i.e., which is returned as a reflected signal from the surrounding environment. Through some signal processing algorithms (usually, Fourier transform-based), it is then possible to estimate the distance, angle, velocity, and, to some extent, the shape of the targets. TX and RX are usually co-located within the same device: the transmitter sends a first version of the modulated signal and the receiver detects its back-scattered copy from the surrounding environment, after a very short time delay.

Modern radar systems utilize two main *wave functions*; pulsed wave (PW) and frequency-modulated continuous wave (FMCW). While radars are traditionally used to detect and track objects that move in the far field, such as vehicles and airplanes, here we are concerned with indoor or city environments where the objects to be tracked may be cars or humans. Moreover, besides the tracking, vital signs can also be monitored such as the breathing rate

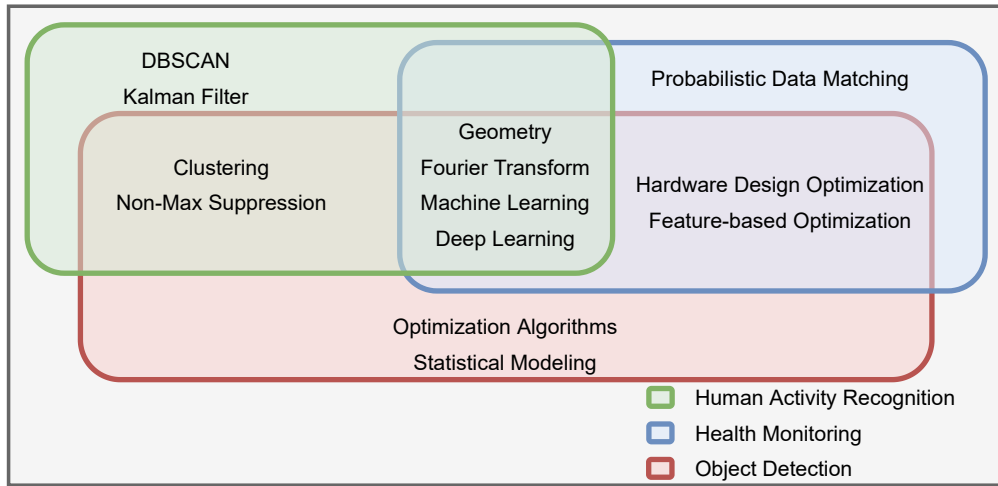


Fig. 8. Overview of techniques used for mmWave radar sensing applications.

and the heart rate. Although these recent applications share common features with traditional (far field) approaches, they also exhibit major differences due to the short distance of the radar from the targets (near field).

B. Pulsed Wave Radar

With PW radars the electromagnetic waves from an antenna are emitted in short bursts. The logic behind PW is to wait for the reflections from the previously transmitted signal to reach to the antenna before sending the next burst. Thus, the reflected signal from the initial emitted sequence of pulses are sampled via a secondary sequence of pulses with a different repetition time. In PW radars, energy of the transmitted pulse is relatively small due to the limited peak amplitude. This limitation in amplitude together with sequential sampling limits the dynamic range and results in a relatively poor SNR at larger distances. For these reasons, PW-type radars have fallen out of favor, and are not used for the applications that will be discussed next, which are mainly about object and people detection, tracking/identification, and vital sign monitoring. From the next section onward, we thus concentrate on FMCW systems, which typically are the technology of choice for medium and larger ranges. Still, for short range applications, such as gesture tracking, PW-type radars might still be a viable alternative.

C. Frequency-Modulated Continuous Wave Radar

As the name implies, FMCW radars transmit a frequency-modulated signal in a continuous fashion. Due to the larger temporal duration of continuous-wave signals, FMCW yields a much larger energy on the emitted signal as compared to PW. In order to cover the desired frequency band, the signal is linearly modulated over time starting from the lower frequency within the band to the higher frequency (or vice-versa). This type of signal is most frequently referred to as a chirp, and the linear modulation of the signal is called frequency sweep. An analogue continuous-wave signal can be generated with a voltage-controlled oscillator (VCO), providing flexible adjustments to the sweep duration independent of the bandwidth. A frequency synthesizer together with a VCO can be used to provide a digital alternative. This technique also provides a higher spectral purity which makes it possible to avoid accidental emission of frequencies adjacent to the desired band, and thus to comply with given regulations. In FMCW radars, the received signal is multiplied by the TX signal. The intermediate-frequency signal component that results is then isolated via low-pass filtering. Additionally, a low-cost ADC can be used to convert the received signal into the digital domain. Due to the recent developments on radar hardware, the wider operating frequency range and the above mentioned advantages, FMCW radars are currently preferred over PW ones, especially in millimeter-wave band applications.

FMCW Signal: As previously mentioned, a chirp is a linearly modulated FMCW signal: it is a sinusoidal function formulated as $\mathbf{x}_{tx} = \sin(\omega_{tx}t + \phi_{tx})$, where the frequency $f_{tx} = \omega_{tx}/(2\pi)$ increases linearly over time. After transmission, the reflected chirp signal from an object is collected at the RX antenna and can be written as $\mathbf{x}_{rx} = \sin(\omega_{rx}t + \phi_{rx})$. The intermediate-frequency (IF) signal is produced by mixing RX and TX signals in the mixer component of the radar as $\mathbf{x}_{if} = \sin((\omega_{tx} - \omega_{rx})t + (\phi_{tx} - \phi_{rx}))$. The time delay between the RX and the TX signals is $\tau = 2d/c$, where d is the distance to the objects and c is the speed of light in air. The start of the

IF is at τ , which is also when RX chirp is realized and ends when the TX chirp is entirely transmitted. Time delay is the foundation for computing the range and velocity of a target in an environment. While the given introductory FMCW concepts are sufficient for the purpose of this paper, further details on FMCW radars can be found in [141].

Range Measurement and Resolution: Range resolution is defined as the ability of a radar to identify closely packed objects. When the distance separating two objects is smaller than the resolution, the radar becomes unable to distinguish between them, returning a single range reading. The range measurement is carried out by computing the phase difference between TX and RX chirps, yielding the initial phase of an IF signal, that is formulated as $\phi_0 = 2\pi f_c \tau$, where $f_c = c/\lambda$ stands for the frequency, c is the speed of light and λ is the wavelength. Hence, the distance d to an object, the so called range $d = \tau c/2$, can be retrieved as $d = \phi_0 c/(2\pi f_c) = \phi_0 \lambda/(4\pi)$. When multiple objects are present, a single TX chirp results in the reception of multiple reflected (RX) signal copies. According to the different time delays (τ) between the TX and each of the RX chirps, multiple IF signals are computed, and range measurements for each corresponding object are derived. The range resolution $d_{\text{res}} = c/(2B)$, highly depends on the bandwidth B of the radar [142]: it can be improved by increasing the bandwidth swept by the chirp, yielding a longer IF signal and, in turn, leading to a more precise reading of the environment.

Velocity Measurement and Resolution: In an FMCW radar the velocity computation (commonly referred to as Doppler) can be achieved using two TX chirps. Initially, the object range is calculated by applying a fast Fourier transform (FFT) to the RX chirps. This range calculation is commonly called range-FFT. The range-FFT of separate chirps at the same location will yield different phases. The object velocity is then derived according to the phase difference between the two chirps as $v = \lambda \Delta\phi/(4\pi T_c)$, where $\Delta\phi$ is the phase difference and T_c is the chirp duration. However, in the case of multiple moving objects having the same distance from the radar, the above method no longer works. To overcome this, the radar needs to transmit N chirps with equal separation, i.e., a so called *chirp frame*. When the chirp frame is passed through the range-FFT, it yields a phase difference containing combined phase differences of all the moving objects. The result of the range-FFT is passed through a second FFT called Doppler-FFT to identify specific phase differences ω of each object. In the case of two objects, the corresponding phase differences, ω_1 and ω_2 , can be used to derive two velocities as $v_1 = \lambda \omega_1/(4\pi T_c)$ and $v_2 = \lambda \omega_2/(4\pi T_c)$. The velocity resolution, v_{res} , of the radar is inversely proportional to the duration of a single frame, $T_f = NT_c$. By knowing the frame duration T_f , the velocity resolution is $v_{\text{res}} = \lambda/(2T_f)$ [142].

Angle Measurement and Resolution: In radar sensing applications, most often the “angle” refers to the horizontal-plane AoA at the receiver (or *azimuth* in a spherical coordinate system). It is calculated by observing the phase changes occurring on the range-FFT or Doppler-FFT peaks. In order to observe these changes, there have to be at least two RX antennas. The difference between the readings of each antenna is what produces the phase change in the FFT peaks. The phase change is formulated as $\Delta\phi = 2\pi \Delta d/\lambda$ s.t. $\Delta d = \ell \sin(\theta)$, where ℓ is the distance between the antennas. Accordingly, the angle can be estimated as $\theta = \sin^{-1}(\lambda \Delta\phi/(2\pi \ell))$. The closer θ is to zero, the more accurate the angle estimation becomes. In fact, the angle resolution $\theta_{\text{res}} = \lambda/Nd \cos(\theta)$ is usually given

TABLE VIII
SUMMARY OF THE HARDWARE PLATFORMS USED IN THE LITERATURE

Hardware platform	Related literature
Google SOLI	[143]
Infineon SiGe	[144]
INRAS RadarLog	[145]
Keysight EXG N5172B	[146], [147]
Qualcomm 802.11ad device	[148]
TI AWR1243	[149]
TI AWR1443	[150]–[153]
TI AWR1443BOOST	[152], [154]
TI AWR1642	[155], [156]
TI AWR1642BOOST	[157]–[160]
TI AWR1643BOOST	[161]
TI AWR1843BOOST	[162]
TI AWR2243	[163]
TI AWR6843	[164], [165]
TI IWR1443	[166], [167]

assuming $\theta = 0$ and $d = \lambda/2$ which simplifies it to $\theta_{\text{res}} = 2/N$. The field of view of the radar depends on the maximum AoA that can be measured [142].

We remark that the distance and angle resolution of a mmWave radar device are especially important as they characterise the density and the minimum separation of the points that are detected in the radar maps (see next section). This, in turn, has a major impact on the resolution of the clustering algorithms that are used to separate signals reflected by different subjects and objects in the radar maps (see, e.g., density-based spatial clustering of applications with noise (DBSCAN) in the following sections) and, on the final tracking performance of any signal processing pipeline.

In Table VI-C, we summarize the types of passive mmWave radars employed in the literature covered by our survey. We observe that the availability of commercial evaluation boards from Texas Instruments (TI) and of software interfaces enabling the retrieval of raw radar data has made TI devices the platforms of choice in many of the works. However, others still prefer powerful but less commercial devices or come up with custom boards when commercial platforms are not sufficient to satisfy the requirements of the application.

D. Key Processing Techniques

Next, we describe some key processing techniques that are utilized in modern mmWave based radar systems. As detailed below, these are used for various purposes such as noise removal, object/people tracking, people detection and identification, vital signal estimation, etc. Note also that multiple techniques are often used concurrently as part of the same solution. By processing distance, velocity and angle information, it is possible to get two or three

dimensional data points, such as *range-Doppler* (RD), *range-azimuth* (RA) or *range-Doppler-azimuth* (RDA) maps. This type of data shape, with temporal information between the data frames, can be further processed to provide valuable information about objects and users in positioning, tracking and identification applications.

micro-Doppler — In addition to the main (bulk) movement of an object, it is possible to have mechanical vibrations within the object body as well. These internal vibrations are called *micro motions*. The micro-Doppler phenomenon is observed when these micro motions from the object cause a frequency modulation on the returned signal [168]. An example for this would be the individual movements of the legs and the arms of a person while walking, or rotations of the propellers of a fix-winged aircraft while flying. Assuming that the scalar range from the radar to an object is $r(t)$ and that the carrier frequency is f_c , then the phase of the baseband signal is defined as $\phi(t) = 2\pi f_c \frac{2r(t)}{c}$. With this, it is possible to obtain the micro-Doppler frequency shift caused by the motion of an object. Taking the time derivative of the phase yields $\frac{d}{dt}\phi(t) = 2\pi f_c \frac{2}{c} \frac{d}{dt}r(t)$. We manipulate this equation by introducing the Doppler shift induced by the rotation of the object and referring to vector \mathbf{p} as the location of an arbitrary point on it. Thus, the micro-Doppler frequency shift equation is obtained as $f_D = \frac{2f}{c}(\mathbf{v} + \boldsymbol{\Omega} \times \mathbf{p})^T \cdot \mathbf{n}$. The first term of the equation is the Doppler shift due to the object's translation $f_{\text{trans}} = \frac{2f}{c}\mathbf{v} \cdot \mathbf{n}$, where \mathbf{v} is the bulk velocity of the object and \mathbf{n} is the radar's line of sight direction. The second term is the Doppler shift due to the object's rotation $f_{\text{rot}} = \frac{2f}{c}(\boldsymbol{\Omega} \times \mathbf{p})^T \cdot \mathbf{n}$, where $\boldsymbol{\Omega}$ is the angular velocity of the object. In order to get time-varying frequency distribution of micro-Doppler modulation, the short-time Fourier transform (STFT) [169] is used. STFT is a moving window Fourier transform where the signal is examined for each window interval in order to generate a time-frequency distribution. This process can be pictured as a DFT multiplied by the sliding window's spectrum, which yields a spectrogram of time-varying micro-Doppler modulation [170], [171]. Due to the different characteristics in micro-Doppler, it is possible to detect a moving body and even to identify it, by capturing the particular modes of motions of the body parts.

Kalman filter (KF) — It is a key tool for the analysis of time-series containing noise or inaccuracies, providing a precise understanding on how the signal changes with time. The KF estimates the *state* of the monitored process through time, by removing random noise. It is commonly used in movement control, navigation and activity recognition, and it is as well widely employed in radar applications. The discrete KF (DKF) was initially developed in [172]. It is a two-step recursive algorithm. The first step of the recursive loop is the *prediction* step, where a projection from the current state of the model and corresponding uncertainties into the next time-step is made. Second, the *correction* (or update) step is where adjustment of the projection is made by taking the weighted average of the projected state with the measured information. In linear systems with additive Gaussian noise, DKF works as an optimal least-square error estimator. While for non-linear systems, the most common KF variants are the EKF and the UKF. One of the possible ways of obtaining state estimations in non-linear models is converting the system into a linear one. At each time step, the EKF uses a first-order partial derivative matrix for the evaluation of the next predicted state starting from the current one. This essentially forces the system to use *linearized versions* of the model in the correction step [173]. However, when the model is highly non-linear, the EKF could experience very

slow convergence to the correct solution. In such non-linear models, the KF is used with an unscented transformation and hence the derivation of UKF. In order to carry out predictions, the UKF picks a finite set of points (called sigma points [174]) around the mean and generates a new mean by passing this set through the non-linear function that describes the system. Thus, the new estimate is obtained. While the computational complexity of both filters are same, for most cases the UKF practically runs faster as compared to the EKF, as it does not calculate partial derivatives [175].

In radar systems, the KF makes it possible to reliably estimate the trajectory of the targets, which is achieved by filtering the temporal sequences of points in the RD, RA or RDA maps, by identifying the center of mass (COM) of the moving target(s) and estimating its (their) trajectory (trajectories) over time. KF allows coping with random noise, obtaining robust trajectories, and to also estimate tracks for the targets in those cases where some temporal RD/RA/RDA frames are lost due to occlusions see, e.g., [145]. Given the sampling time of radar applications and the typical speed of movement of people, linear KF models are usually appropriate for human trajectory tracking. Also, most prior works use KF to track the COM of an object or person, treating it as an idealized point-shaped reflector.

A recent solution for mmWave indoor radars [176] uses an extended object tracking KF, which makes it possible to jointly estimate the COM and the *extension* of the target around it. In [176], such extension is mapped onto an ellipse around the COM, whose shape and orientation matches those of the target. This KF technology has similar performance as standard KF assuming point-shaped reflectors in terms of tracking accuracy for the COM, but *additionally it makes it possible to track the object extension over time*. In the case of human sensing, the ellipse represents the way the torso is oriented within the monitored environment. This information, combined with the target trajectory, reveals where the target is steering at, which may be a valuable information for some applications, e.g., for the retail industry.

E. Main learning techniques

Nowadays, machine learning (ML) and especially deep learning (DL) is being applied to many different fields and applications. Although most of these techniques have been around for a long time, they are recently emerging due to hardware advancements. ML methods are used for regression, classification and clustering tasks. A more comprehensive analysis and discussion of ML and DL techniques are respectively given in [177] and [178]. Just like many other fields, these techniques are being successfully and abundantly exploited within mmWave radar sensing systems.

In some cases, it is required to group sets of objects into categories, i.e., to perform *clustering*. This technique is widely used in such areas as pattern recognition, image analysis and machine learning. This is particularly relevant when there are scattered data points in the observed space, and the information about which point belongs to what category is non trivial. In our setup, it is used for the analysis of radar images. After the cluster analysis, if the results are good, the clustering method could be exploited to compute labels on the dataset, and it could even be used as a part of a more sophisticated system, e.g., for a subsequent identification of the subject or of the human that has generated each data cluster within an image. Often, the clustering task is carried out in an *unsupervised*

fashion. Over the years, many researchers have designed clustering algorithms tailored for a variety of models. Some of the well known of clustering algorithms are *k-means* (based on partitioning), *AUTOCLASS* (based on Bayesian statistics), *expectation maximization* (EM) (based on parametric statistics) and also unsupervised neural networks and DBSCAN [179] (density based). More on the existing clustering models and algorithms, their categorization and discussion can be found in [180].

DBSCAN — Considering the data gathered by mapping the radar signal on the environment are tightly packed points in range, angle and velocity dimensions, one algorithm stands out in the field of radar sensing, density-based spatial clustering of applications with noise (DBSCAN) [179]. DBSCAN is a density-based clustering technique where the points belonging to a high density region are grouped discarding those that are recognized to be isolated, in accordance with precise definitions of the neighborhood of a point and of its local density. The algorithm starts at an initial point featuring a dense neighborhood and tags it as a *core* point. The remaining points within the *core* point's neighborhood, i.e., within a preset radius from it, are referred to as *reachable*. Upon initializing the first *core* point, DBSCAN evaluates the neighborhood density of each *reachable* points within its neighborhood, and the ones residing within a dense neighborhood are chosen as the new *core* points. The *density connected* region of the cluster is thus extended by connecting dense neighborhoods, constructing clusters of generic shapes and only containing densely connected points. This process is continued in a recurrent fashion until there are no more *reachable* points whose neighborhood exceeds the minimum density. Finally, a cluster is defined as the collection of all points that are either density-connected or density-reachable. Multiple clusters are possible and represents density-connected regions of points. Points that are not contained within a high-density cluster are referred to as *outliers* (these are termed noise points, and are rejected).

In mmWave based radar applications, DBSCAN has been extensively and successfully used to extract the clusters of data points in the RD, RA or RDA maps associated with the tracked humans and/or objects (e.g., vehicles) in the monitored environment [181]. This technique was found to be very robust and efficient due to the following reasons: i) most importantly, DBSCAN is an unsupervised method, its simplest version only needs two parameters to work (a density threshold and a radius for the density neighborhood), while it does not need one to know in advance the number of clusters (objects/humans) to be tracked. The DBSCAN parameters are to be set at training time and, for given hardware (mainly, working frequency, distance and angle resolution) and environment choices (e.g., indoor vs outdoor), their set values remain rather effective across a large number of scenarios [145], ii) DBSCAN runs fast, with a time complexity of $\mathcal{O}(n \log n)$, where n is the number of points to be evaluated, iii) the clusters do not have to be spherical, DBSCAN works well with clusters of any shape and it is very effective in rejecting random noise, which is quite common in radar maps. Further discussion on how DBSCAN is used in radar systems and applications from the state-of-the-art is presented in Section VI-F.

Neural networks — The term *neural network* (NN) comes from biological processes where a collection of neurons create a network. In the modern sense, NNs are the technology counterpart of the brain. They try to achieve learning by identifying the relationships in a set of data similarly to how brain does [182]. The most basic

NN is the perceptron originally devised by Rosenblatt [183]. It only has a single layer and performs a classification task based on taking the input and multiplying it by given weights, summing the resulting signals, and passing the result through a non-linear decision function. Essentially, this is the idea behind the whole DL field. Below, we talk briefly about some state-of-the-art DL architectures, which have captured the attention of researchers working on radar sensing applications.

Convolutional NNs (CNNs) — One of the most common NN models is the CNN [184]. CNNs usually consist of back to back convolutional and pooling layers with a final fully-connected layer. The convolutional layers take the input and process it via a kernel function (a filter) where the feature detection is carried out. These feature maps are then fed to the pooling layer where dimension reduction of the domain is performed. This process is continued until a fully-connected layer, where a flattened feature map is computed and used to obtain the classification output (either via a single non-linearity or a softmax layer). CNN is a feedforward NN where information can only move in the forward direction from the input to the output layer, without cycles nor loops. While the convolution operation is naturally invariant with respect to rigid translations of input patterns, it does not work with other types of transformations, such as rotations. For this reasons, in the radar sensing field dedicated CNN-based approaches have been specifically proposed for radar point clouds, which are discussed shortly below.

Use with mmWave radar signals: due to the lack of mathematical models to describe RD/RA and RDA maps from mmWave radars and to the presence of strong noise components (e.g., from ghost reflections and metallic objects), CNN have been extensively used to automatically obtain meaningful feature representations from radar readings. Usually, CNNs are applied to the RD/RA/RDA clusters found by a preceding clustering algorithm, e.g., DBSCAN, assuming that each cluster represents a target object within the monitored space. These representations can be then utilized to detect objects within an environment [185], to assess the type of activity a person is carrying out [155], or to even track their identity [145].

Recursive NNs (RNNs) — Unlike feedforward NNs, RNNs [186] utilize their internal memory to retain information from previous input samples. This allows temporal sequences to be used as input and thus the learning process can extract temporal correlation. Hence, RNNs remember the information during the learning process, while feedforward NNs cannot. This is especially relevant for radar data, as it makes it possible to extract temporal features from a sequence of radar maps (i.e., a trajectory). For example, such features can describe the way a person moves his/her limbs while performing a certain activity. Vanishing or exploding gradients are commonly seen during the back-propagation [178] based training of an RNN. This prevents the NN to effectively learn, leading to a premature stopping of the training process. Long-short term memory (LSTM) cells, or alternatively gated recurrent unit (GRU) cells [187], extend the original RNN neuron to effectively cope with vanishing or exploding gradients [188], by intelligently redefining the structure of a memory unit. This solves the gradient vanishing problems at the cost of a greater complexity.

Use with mmWave radar signals: activity recognition usually cannot be achieved on data coming from a single

time step, e.g., from a single RD/RA or RDA map. For an activity to be determined, analysis of a sequence of such radar maps should be carried out. Combining this with the micro-Doppler effect observed in humans, it is possible to estimate the identity of a person based on the specific micro motions of their body parts [145], [176], [189].

Autoencoders (AEs) — Autoencoders [190] encode the input and then decode it to generate the output. While an AE is trained to copy the input onto the output, the main rationale behind this is to learn internal representations (features) that describe the manifold where the high-dimensional input signal resides. That is, the AE features should be highly representative of the input and can be used to classify it with high accuracy. For a proper training of the AE, the encode/decode functionalities are constrained, e.g., by limiting the number of neurons in the inner layer or forcing some sparsity for the inner representation. This forces the AE network to approximate the output by preserving the *most* relevant features. Denoising autoencoders [190] are trained to denoise the input signal and reconstruct, at their output, the original (noise-free) signal version. This was found to produce better features in the AE inner layers. In addition, the denoising capability of such NN architectures is valuable for RD/RA/RDA radar maps due to their noisy nature.

Use with mmWave radar signals: radar system are prone to noisy data and can be significantly affected by unwanted or fake reflections (e.g., ghost reflections). Due to this, many radar applications use the AE encode/decode functionalities as a middle ground for the reconstruction of the desired observation such as anomaly analysis for human fall detection [162], person detection for surveillance systems [191] and indoor person identification [145].

Generative adversarial networks (GANs) — In general, GANs [192] are divided into two sub-models called the *generator* and the *discriminator*. In the *generator* network the expected outcome is a newly generated sample which should reflect the features found in the input data/domain. Conversely the task of the *discriminator* network is to classify an input to detect whether it is a fake (generated) or a real example. Learning proceeds as a game, where the generator becomes progressively better in generating fakes, and the discriminator improves at detecting them. The final goal is again to learn meaningful representations (features) of a (usually) high-dimensional input signal.

Use with mmWave radar signals: Because of the competitive nature of the generator and discriminator networks, jumping from one to another during training makes them better at their respective tasks. Most often, algorithms exploit this fact to generate the required data and use this newly generated input whenever it fits. For instance, GANs have been used in [150] to generate dense maps from sparse inputs (also referred to as super resolution imaging) for the purpose of environment mapping in a low-visibility environment. In this case, the generator network is used to improve the image resolution and the discriminator to train the generator better.

Residual networks (ResNets) — ResNets [125] use shortcuts to skip layers. Typically, the skipped layers include activation and batch normalization [193]. The reason behind using shortcuts is to overcome vanishing gradients and/or gradient degradation problems. Despite the seemingly simple architectural change, this leads to a major change in terms of learning paradigm, which preserves the correct propagation of the error gradients across the whole network, allowing one to build very deep networks with hundreds of layers and with a remarkable representation

(feature extraction) effectiveness.

Use with mmWave radar signals: Due to the large number of layers that can be stacked, ResNets are exploited in complex scenarios where the input signal contains a high number of patterns to be concurrently classified. Examples include human skeletal posture estimation [158], where the detection of more than 15 joints and the subsequent tracking of the person are carried out, or real-time object detection for autonomous driving [185], where real time obstacle detection is performed.

PointNet and PointConv — Images are represented through dense regular grids of points, whereas point clouds are irregular and also unordered. For these reasons, using the convolution operation with them can be difficult. Pointnet [194] is a deep neural network which uses unordered 3D (graph) point clouds as input. The applications of PointNets are object classification and semantic segmentation. An extension of this network is Pointnet++ [195], where the PointNet architecture is recursively applied on a nested partitioning of the given point cloud. PointNet++ can identify local features on a greater contextual scale. The key reason of using such architecture is to make the extracted features *permutation invariant* with respect to the input signal. Along the same lines, in [196] the convolution filter is extended into a new operation, called PointConv, which can be effectively applied to point clouds to build convolutional neural networks. These new network layers can be used to perform translation-invariant and permutation-invariant convolutions (and obtain invariant features) on any point set in the 3D space. These qualities are especially important for radar point clouds. When tracking people or objects from radar data, being rotation invariant is relevant as the traits that we want to capture about the target (movement of limbs, body shape, etc.) do not depend on their orientation in space.

Use with mmWave radar signals: In the recent papers [176] and [197], novel Pointnet based NNs are presented to track and identify people from point clouds obtained by mmWave radars. We remark that mmWave systems can either operate on dense radar Doppler maps, or on point clouds which can be derived from these dense maps by only retaining the most significant (strongest) reflections. Point clouds are less informative, as some information is lost when moving from dense to sparse representations, but are on the other hand easier to store, transmit and their processing is also lighter. For these reasons, algorithms that operate on sparse point clouds are particularly appealing and are gaining momentum.

F. Selected Applications

Some of the works that we review in this section adopt a custom design for the whole sensing system, from the radar hardware to the implementation of the software. Others, instead, use off-the-shelf radar devices and present new algorithms. Most of the applications deal with human activity recognition, object detection and health monitoring, but other use cases are emerging such as vibration detection, environment mapping and even speech recognition.

Human Activity Recognition

For the purpose of tracking and identity recognition of humans moving in a room, the authors of [145] use micro-Doppler signatures obtained from back-scattered mmWave radio signals. An off-the-shelf radar is used to gather RDA maps and noise removal is carried out. Hence, DBSCAN is applied to the pre-processed RDA maps to detect the data points (signal reflections) generated by each of the human targets in the monitored environment. With DBSCAN, a cluster of RDA points is obtained for each subject and updated as the targets move, across subsequent time steps. Trajectory detection is carried out by applying a Kalman filter to the clusters and, as a final step, identity recognition is carried out using a CNN with inception layers. The average accuracy is of 90.69% for single targets, 97.96% for two targets, 95.26% for three targets and 98.27% for four targets.

Similarly, in [155] micro-Doppler signatures are extracted and exploited for human motion detection, where both RD data cubes as a whole, and RD point clouds are considered. The real-time information is received by passing RD data through Doppler-time extraction. DBSCAN is used to group the RD point cloud data from each of the tracked users in the monitored space. The movements of arms, torso and legs of a walking person are then identified via a CNN model. Tests were carried out for walking and leaving, waving hands, sitting to walking transition, walking back and forth, and combining all behaviors. An average accuracy of 96.32% (walking), 99.59% (leaving), 64% (waving hands), 91.18% (sitting to walking), 97.84% (walking back and forth) and 95.19% (all) was observed for each scenario, respectively.

In the same vein, movement pattern detection for of one or two patients is the key result in [157]. Together with DBSCAN, Kalman filtering has been applied to track the trajectory of each patient. Walking, falling, swinging, seizure and restless movements are the movement patterns which are classified by the proposed CNN model. For these movement types, the authors have obtained accuracy values ranging between 82.77% and 95.74%.

The authors of [146] have proposed a framework called “mmSense”. It uses an LSTM-based classification model for localization. Initially, environment fingerprinting is carried out with and without human presence. Hence, the presence of people and their location within the environment are estimated using an LSTM model. Moreover, an approach combining human outline profile and vital sign measurements gathered from 60 GHz reflected signal strength series is devised to identify the targets. mmSense was tested on five people concurrently sharing the same physical space, achieving an accuracy of 97.73% for classification and of 93% for identification tasks, respectively.

With the purpose of preventive decision making in autonomous driving applications, the authors of [158] propose “mm-Pose”, a model for estimating the posture of a person in real-time. To achieve this, RDA data is used to obtain 3D cloud point representations and red-green-blue (RGB) projections of depth-Azimuth and depth-Elevation are used. CNN is used to cope with noise and unwanted reflections and also to detect skeletal joint coordinates. The final model was able to locate 17 human skeletal joints with errors of 3.2 cm, 2.7 cm and 7.5 cm on the depth, elevation and azimuth axes, respectively.

A similar application is presented in [161] for human skeletal pose estimation. In this model, range-angle heatmaps are initially fed to a CNN followed by a fractionally strided convolutional network (FSCN). To exactly locate the target points, the non-max suppression algorithm was used and the obtained key points were combined, implementing and testing the proposed solution on single user scenarios. The evaluation metrics used in this work are object keypoints similarity (OKS) and Mean Average Precision (AP) over different OKS thresholds. The authors obtained

an average OKS of 70.5 over eight different body parts. As a comparison, camera based pose estimators achieve higher performance, i.e., Openpose (avg. OKS: 93.3) and Leave One Out (avg. OKS: 66.6).

In [162], a fall detection framework, called “mmFall” is presented. 4D cloud points are used, i.e., range, azimuth angle, elevation angle and Doppler. To perform fall detection, the authors exploit a sequence-2-sequence hybrid variational RNN autoencoder (HVRAE) model that utilizes an encoder/decoder logic. They use a tailored loss function along with a simplified version (HVRAE_SL) for testing purposes. They also test the model on vanilla Recurrent Autoencoders (RAE). Overall, HVRAE achieved 98%, HVRAE_SL had 60% and vanilla RAE had 38% probability of detecting a fall.

The authors of [154] designed a system to classify static hand gestures, namely, palm facing the radar, hand perpendicular to radar and thumbs-up gesture. In addition to the real data, artificial reconstructions of the gestures were used to gather synthetic data. Tests were performed both on range and RA maps and, 85% and 90% accuracy were respectively achieved with them, while with the addition of synthetic data, the accuracy increased up to 93.1% and 95.4% for range and RA maps, respectively.

A framework for human detection and tracking by using radar fusion is presented in [152]. Ground truth data is obtained via a camera system. DBSCAN is used for clustering and temporal relationships between clusters are exploited to obtain the probability distribution of the new positions to perform tracking, similar to Kalman filtering. The concurrent use of two radars allows improving the accuracy from 46.9% to 98.6%.

The “GaitCube” algorithm was proposed in [151]. It utilizes so called gait data cubes, i.e., 3D joint-feature representations of micro-Doppler and micro-Range signatures for human recognition purposes. The idea behind this algorithm is to exploit the radar’s multi-channel capabilities to improve the recognition accuracy. Their proposed system achieves 96.1% accuracy with a single antenna, 98.3% when using all antennas and an average accuracy of 79.1% when tested in an environment not seen at training time.

Akin to the objectives of the above paper, [165] develops a posture estimation algorithm using DBSCAN to cluster and single out real targets. The authors generate their dataset by installing the radar on the ceiling, and receiving data at 10 frames per second. The data processing model is based on CNNs, and the CNN network is trained on lying, seated and upright moving postures. Classification results demonstrate a mean accuracy of 99.1% and an average processing time of 0.13s.

Another work in [156] performs the classification of 7 fitness exercises. CNN and LSTM neural network models are utilized for the classification task, by training them on RD, RA, angle-Doppler (AD) and joint-image data. For these data types, a classification accuracy of 92.08%, 98.65%, 97.7% and 99.27% is attained, respectively. In [153], fitness activities were tested both in offline and also in online scenarios. Classification was performed on 5 human activities achieving an accuracy of 93.25% and 91.52% for the offline and online operation modes, respectively. The system was also tested on multiple locations and the obtained average accuracy is 88.83%.

Authors of [166], [167] have created a human detection and tracking algorithm by using two radars simultaneously. In both of these works, Kalman filter and DBSCAN were used for tracking and identifying the location of the person, and the synchronization of the radars were carried out in an offline fashion. The results in [167] show a significant improvement when a two-radar setup was used with an accuracy of 98.6% compared to 46.9% from single-radar

setup in human detection. In [166], radars were placed so that one had a top-view and the other had side-view angle. This work in addition to prior work proposes an alarm system and a posture estimation method. An alarm system is triggered upon a positive evaluation in the change of cluster number, number of points in the cluster or the center point of the cluster. The posture estimation is done for standing, sitting and lying poses by analysing the height of a person at a particular instance and the accuracy of estimation is from 92.5% to 93.7%.

Object Detection

The authors of [185] propose a method called spatial attention fusion (SAF) for obstacle detection with mmWave radar and vision sensors. A fully connected one-stage (FCOS) NN is used for the detection of objects. For the training of this neural network, radar data is converted into radar maps (images) and during the feature extraction step, the SAF block within the FCOS network is used for combining radar with vision features. The proposed SAF-FCOS model is trained and tested on the nuScenes dataset with a ResNet-50 backbone, achieving an average precision of 90.0% with an intersection-over-union of 0.50 or higher.

The detection of concealed objects implies additional challenges, as it becomes necessary to single out hidden objects from rest of the scenery. In [198], the authors employ EM to fit a Gaussian mixture model of the image acquired: through a two-step image segmentation procedure, they first extract the body area from the image and then detect concealed objects. The model is evaluated in terms of average probability of error and the authors report that multi-level EM has an increased performance of up to 90.0% when compared to conventional EM.

A real-time outdoor hidden object detection model is proposed in [199]. This work also utilizes EM, Bayesian decision making and Gaussian mixture model for image segmentation, with an architecture similar to that of [198]. However, vector quantization is adopted for the first segmentation level to achieve faster computation times. The authors also state that EM can be avoided as a whole to reduce computation time (and complexity) significantly, but this causes an error increase as well. As a result, [199] achieves a computation time of 1.11 s (with EM) and 0.134 s (without EM) per frame.

Along a similar line, the authors of [200] propose a writing object (e.g., a pen) tracking system called “mTrack,” that uses dedicated mechanisms to suppress interference from background reflections. After this, the RX antenna is steered according to the peak response observed on the reflected received signal. In other words, the antenna is adaptively steered to face and track the direction of the pen. Finally, the target movement tendency is evaluated by the trend and amount of phase shifting. The system can detect the location of the pen at a 94% accuracy, with a tracking error smaller than 10 mm across 90% of the trajectory.

In [201], a non-imaging sensor for hidden object detection is developed. The authors test their device both in an outdoor scenario with a gun and in an indoor scenario where plastic sticks of diameter equal to 2 cm are covered by a fabric. Final results of the model are evaluated by applying Fourier transform on IF chirps to get the range map on horizontal and vertical scans of the environment compared with a captured image. In [202], an improved version of the sensor is proposed, using a horn antenna integrated with a focusing dielectric lens operating in the 80–100 GHz frequency range. This sensor can be operated with any preferred movement (e.g., up-down) and the authors claim that the probability of detection can go up to 100%.

In [148], an IEEE 802.11ad device is used as a pulsed wave radar to perform passive handwriting tracking. Slow- and fast-time dimension analysis of the complex CIR, cell-averaging constant false alarm rate (CA-CFAR) and subsample peak interpolation (SPI) are the underlying techniques used in their algorithm. After applying digital beamforming, the authors could extract Doppler maps and by choosing the bins with higher Doppler power, could localize the writing tool (a pen). Finally, the pen is tracked by picking the lowest elevation angle of its lower part at each time-step. With this, they achieved a tracking accuracy between 3 mm (at a distance of 20 cm) and 40 mm (at a distance of 3 m) and a character recognition accuracy ranging from 72% to 82%.

The authors of [203] perform object classification considering three classes: humans, drones and cars. The feature set used in their algorithm consists of radial range, area under the peak, width of the peak, height and standard deviation of the peak in the range-FFT domain. Logistic regression and Naive Bayes led to a classification accuracy of 86.9% and 73.9%, respectively.

In [204], authors have developed a new deep learning model called hybrid dilated convolution (HDC) for concealed object detection. HDC uses two-class semantic segmentation network for keeping a high resolution in order to detect small objects. As a design rule and assignment strategy, expand-contract dilation (ECD) assignment is applied. In this assignment stage, the first dilation rate group forms the “rising edge” (increasing dilation) and the rest forms the “falling edge” (decreasing dilation) of dilation rates. As a result, their average precision with intersection over union of 0.5 is at 0.69% which outperforms rest of the existing techniques.

Health Monitoring

The authors of [205] propose a model for remote heart rate (HR) monitoring and analysis. They use the Levenberg-Marquardt (LM) algorithm for the extraction of heart-rate information. The sum of heartbeat complex, respiration, body movement, background noise, and electronic system noise is gathered by expressing the received in-phase and quadrature-phase components from LM as the cosine and sine of the received signal. One distinctive advantage of this method is that there is no phase unwrapping as the fitting of the HR signal is directly carried out on the cosine and sine of the received phase modulated signal, which is important for low SNR scenarios. The method is able to estimate beat-to-beat HR and individual heartbeat amplitude, both having a critical role in the diagnosis of heart diseases.

The authors of [149] demonstrate a remote breathing and sleep position monitoring system over multiple people at the same time. High resolution AoA detection is used to identify closely located targets. A support vector machine (SVM) is used for finding the sleep position, and an optimal filter to estimate the breathing rate. The designed system achieved an accuracy of 97% for breathing rate estimation and of 83% for sleep position detection.

In the same vein, the work in [147] proposes vital sign and sleep monitoring system. Initially, the location of the person is detected by using the reflection loss as the classification parameter, performing a 360° sweep of the environment. After localizing the human, reflected signal strength samples from the reflected signal directed at the human are gathered. For heart rate detection, FFT, customized band-pass filter, inverse FFT (IFFT) and peak detection are applied, while for breathing rate detection only IFFT and peak detection were sufficient. The achieved accuracy was 98.4% and the mean estimation error in breathing rate and heart rate estimation for an incident angle

of 70° was smaller than 0.5 bpm and 2.5 bpm, respectively.

A similar purpose is found in [164], which designs a robot for human detection and heart rate monitoring. The Hungarian Algorithm and Kalman filtering are used to detect and track the user position. Once the person is located, the robot approaches him or her and starts the scanning process. The biquad cascade infinite impulse response (IIR) filter is used to extract the heartbeat waveforms from the signal, whereas a NN is used for predicting the heart rate. The proposed system achieved an accuracy between 91.08% and 97.89% across eight different poses.

For the purpose of remote glucose level monitoring, the authors of [143], [144] observe reflected multi-channel signal signatures collected through the SOLI mmWave sensor [206]. The signal is analyzed by obtaining average power spectral density (PSD) of each gated signal vector by applying DFT and FFT. With this, they were able to sense the change in dielectric constant due to a varying glucose level in the blood.

The authors of [163] use the radars' multi-channel capabilities to improve the estimation of vital signs (heart rate). Experiments are performed on 4 different scenarios by changing the location of the radar and the posture of the subject. Authors claim that using multi-channel Maximal Ratio Combining (MRC) outperforms single channel estimates in most cases, quantifying the benefits for each scenario.

Other Applications

In [159], a system namely “mmVib” for micrometer level vibration detection is presented. The authors propose a multi-signal consolidation model to understand In-phase and Quadrature (IQ) domain and in turn exploit the consistency among the two obtained signals to estimate the vibration characteristics of an object. With this, they can detect vibrations at micrometer level.

The authors of [150] propose an indoor mapping system called “milliMap”, designed for low-visibility environments. A lidar is used for environment mapping as a ground truth data collector. A GAN is used to construct the grid map by recognizing obstacles, free spaces and unknown areas. Finally, semantic mapping is applied for the classification of obstacles.

A noise-resistant speech sensing framework, “WaveEar,” is proposed in [207]. Directional beamforming is used to make the system robust to noise. After localizing the throat and receiving the data, voice reconstruction is achieved by a neural network based on an encoder-decoder (autoencoder) architecture. As a result, WaveEar achieves a stable 5.5% word error rate at a distance of about 1.5 m from the user. The authors also point out that joint optimization speech-to-text and WaveEar would further enhance the capabilities of their system.

In [160], a mmWave radar device is mounted on a robot to estimate its position. This is achieved by exploiting the interference produced by other mmWave radars located in the same environment (with known positions), and by only estimating the angle of arrival of each other radar interference. The proposed system attains position errors for the robot ranging from 14 cm (with three radars) down to 6 cm (ten radars).

G. Summary

In this section, we have summarized the recent advances and trends in signal processing for passive mmWave radar systems for indoor spaces. These systems are rapidly gaining momentum as radar devices become commercially available, at a low cost. A number of applications are emerging, targeting diverse scenarios such as people detection, tracking and identification, estimation of biosignals such as respiration and heart rate, detection of gestures/activities/falls, vibrations, speech or environmental mapping. Table IX summarizes these application-oriented propositions, while Table XI categorizes them based on the environment where the experiments were carried out. While early works used standard machine learning algorithms such as expectation maximization and support vector machines, latest developments have been dominated by neural networks. This is clearly evident from Table XII, which presents a summary of the analytical tools discussed in the survey. These are being implemented in their many flavors, and are allowing researchers to obtain good results in scenarios where no analytical models are available. As far as human data monitoring is concerned (e.g., people tracking, activity monitoring, etc.), the key processing algorithms are DBSCAN clustering for the separation of user data in the radar RD/RA/RDA maps and Kalman filtering to reliably track their trajectories. Neural network architectures are evolving from standard CNNs to more advanced convolutions (PointConv and PointNets) that were specifically designed for radar point clouds. Some solutions then use RNNs to capture and exploit the temporal correlation of radar signals. Advanced architectures, such as GAN based, are also being exploited to extract features from radar images.

TABLE IX
SUMMARY OF THE MMWAVE RADAR SENSING WORKS IN THE LITERATURE

Proposition	Tools Used	Band (GHz)	Performance
Human Activity Recognition Algorithms			
Multi-person tracking and identification [145]	Micro-Doppler, DBSCAN, Kalman filter, Hungarian algorithm, CNN	77	Continuous identification of multiple persons with up to 98% accuracy.
Multi-person detection and identification [146]	LSTM-based model, RSS series analysis	60	Multi person classification and identification accuracy of 97.73% and 93% respectively.
Gait-based human recognition [151]	CNN	77	Classification accuracy of 96.1% and 98.3% with single gait cycle, when using single and all receive antenna respectively.
Human detection and tracking [152]	DBSCAN, probability distribution matching, Kalman filter-like algorithm	77-81	Human detection sensitivity and precision of 90% and 98.6% respectively.
Real-time human activity recognition [153]	DBSCAN, CNN, RNN	77	Offline and real-time activity recognition accuracy of 93.25% and 91.52% respectively, over five different human activities.
Hand gesture classification [154]	Deep learning, Signal processing (FFT)	77-81	Hand gesture classification accuracy of 93% and 95% on range and range-angle data respectively.
Human motion behavior detection [155]	Micro-Doppler, DBSCAN, CNN	77	Accuracy of over 90% in detecting various human motion behaviours.
Activity recognition and fitness tracker [156]	Deep learning, CNN	77-81	Classification accuracy of 92.08%, 98.65%, 97.7%, and 99.27% for RD, RA, Angle-Doppler (AD), and joint-image evaluation respectively.

Real-time patient behaviour detection [157]	micro-Doppler, STFT, CNN	77	Over 84.31% prediction accuracy for different behaviors for a single patient. Around 80% prediction accuracy for different behaviors for two patients.
Human skeletal pose estimation [158]	CNN	77	Detection of 17 human skeletal joints with 3.2 cm, 2.7 cm and 7.5 cm localization error on depth, elevation, and azimuth axes respectively.
Human pose estimation [161]	CNN, Fractionally strided CNN	77	Average object keypoints similarity of 70.5 over 8 different parts.
Fall detection system [162]	LSTM, RNN	77	Proposed scheme achieves 98% fall detection rate and outperforms the baseline techniques.
Real-time posture estimation system [165]	DBSCAN, CNN, LSTM, Decision trees	77	Posture estimation with an accuracy of 99.1% at a processing time of 0.13s
Human detection and tracking [166], [167]	DBSCAN, Kalman filters	76-81	Human detection sensitivity of over 90%. Two-radar setup improves precision from 46.9% to 98.6%. Posture estimation precision from 92.5% to 93.7%

Object Detection Algorithms

Handwriting tracking [148]	STFT, CIR, Cell averaging-constant false alarm rate (CA-CFAR)	60	Tracking accuracy of 3 mm to 40 mm and character recognition accuracy of 72% to 82%.
Obstacle detection for autonomous driving [185]	Deep learning, CNN	77	Average precision of 90% with intersection of unions greater than 0.5.
Concealed object detection [198]	Gaussian smoothing filter, expectation-maximization, Bayesian	37.47	Usage of multi-level EM increased performance up to 90% compared to conventional EM.
Real-time concealed object detection [199]	Expectation-Maximization, Bayesian decision making, Gaussian mixture model	94	Computation time of 1.11 s and 0.134 s with reduced processing.
Writing object tracking (mTrack) [200]	RSS, phase change analysis	60	The system tracks/locates a pen with sub-centimeter accuracy in 90% of the cases.
Concealed object detection [201], [202]	FT	80-100	Object detection accuracy up to 100%.
Object classification [203]	FFT, Logistic regression, Naive Bayes	77-81	86.9% and 73.9% classification accuracy using Logistic Regression and Naive Bayes respectively.
Hidden object detection [204]	Semantic segmentation, CNN	60	The proposed expand-contract dilation (ECD) scheme has an average precision (AP@0.5) of 0.69, and outperforms all the existing techniques.

Health Monitoring Algorithms

Blood glucose level monitoring [143]	DFT, FFT	57-64	Remote detection of blood glucose levels by sensing the change in dielectric constant and loss tangent.
Glucose level detection [144]	DTFT, energy-density comparison	57-64	Demonstrates accurate identification of blood glucose levels.
Vital sign and sleep monitoring [147]	RSS, IFFT	60	Human finding accuracy of 98.4% and the mean estimation error in breathing rate and heart rate is less than 0.43 Bpm and 2.15 Bpm.
Breathing and sleep position monitoring [149]	FFT, DOA, optimum filter, SVM	77-81	Accuracy of 97% and 83% for breathing rate estimation and sleep position detection respectively.

Vital sign monitoring [163]	Arctangent demodulation (AD), Maximal ratio combining (MRC)	77-81	Proposed signal processing chain significantly improves the heart rate estimation accuracy in all cases.
Heart rate sensing [164]	Neural networks, Hungarian algorithm, Kalman filter	60-64	Accuracy of 91.08–97.89% over 8 different human poses.
Heart rate analysis [205]	Non-linear Levenberg-Marquardt	94	Capability of estimating beat-to-beat heart rate and individual heartbeat amplitude.
Other Algorithms			
Indoor mapping [150]	GAN	77	Map reconstruction error within 0.2 m. Obstacle classification accuracy of 90%.
Vibration detection [159]	FFT, AoA	77	Median amplitude error of $3.4 \mu\text{m}$ for the $100 \mu\text{m}$ amplitude vibration.
Robot position estimation [160]	AoA, range and doppler FFT	77	Position estimation of the robot with an error below 20 cm.
Speech sensing [207]	SSNR, Neural network	77	5.5% word error rate around 1.5 m distance

TABLE XI
SUMMARY OF THE ENVIRONMENTS IN WHICH THE EXPERIMENTS HAVE BEEN CARRIED OUT

Evaluation	Related literature
Indoors	[143]–[155], [157], [159]–[167], [198], [200]–[202], [204], [205], [207], [208]
Outdoors	[156], [158], [161], [185], [199], [201]–[203]

TABLE XII
SUMMARY OF THE MAIN TECHNIQUES USED IN THE SURVEYED PAPERS

Analytical Tools	Related Literature
DBSCAN	[145], [152], [153], [155], [165]–[167]
Deep learning	[145], [146], [150]–[153], [153]–[158], [161], [162], [164], [165], [185], [207]
Fourier transform	[143], [144], [147], [148], [154], [159], [160], [201], [203]
Hungarian algorithm	[145], [164]
Kalman filter	[145], [164], [166], [167]
Levenberg-Marquardt method	[205]
Machine learning	[149], [165], [203]
Non-max suppression	[161]
Signal processing	[146], [147], [147], [148], [163], [200], [207]
Statistical modeling	[152], [198], [199]

VII. DISCUSSION AND OPEN RESEARCH DIRECTIONS

Our comprehensive review of the state of the art in mmWave localization and sensing shows that a sizeable set of contributions have already covered significant work in this research area. Such works show that current mmWave equipment, even COTS devices, already offer sufficient opportunities to incorporate localization as part of communication processes. Moreover, commercial implementations of mmWave radars are currently very compact,

and cater for precise device-free localization and sensing. However, additional efforts are required to democratize these tasks and make them natively available to vertical applications that rely on mmWave connectivity.

At the current stage of hardware development, fully-custom signal processing algorithms only apply to software-defined radio platforms, where fully-digital transceiver architectures can be available upfront. Conversely, commercial-grade hardware does not give full access to internal signal samples and measurements, requiring more complex processing and often yielding limited performance. For example, while theoretical analysis predicts millimeter-level device localization accuracy and fully digital architectures achieve centimeter-level accuracy, algorithms for commercial-grade mmWave devices typically achieve decimeter-level 3rd-quartile localization errors.

In this perspective, we conclude that the research in the above field would greatly benefit from new-generation standard-compliant mmWave transceiver hardware that also exposes channel state information to external algorithms. While some efforts in this direction have been announced, there is still no such platform available on the market. The same observation holds for hybrid beamforming architectures. While preliminary works exist that exploit these kinds of architectures to improve beam pattern directivity and adaptivity, or to make the 802.11ad SLS operations faster, these architectures could also help localize mmWave devices faster, e.g., by enabling faster angular spectrum scanning. All of the above would be important enablers of a fully integrated device-based sensing and localization system, for which significant research is still needed. The benefits of achieving such a system would be enormous, as a seamless integration of device-based localization and communications would enable multiple network optimizations (such as optimal client-AP associations, predictive re-association before link breakage due to movement or obstacles, or location-aided beam training and tracking), as well as advanced location-based services.

As for passive radar sensing, a number of major advancements are envisaged. First, most commercial low-cost radars incorporate linear antenna arrays, which have limited detection and tracking capabilities. Bi-dimensional antenna arrays would make it possible to detect higher resolution radar images in the 3D space, enabling new uses of this technology (e.g., human gait analysis). Almost no work is available to date exploiting 2D antenna arrays. Second, most of the available research only involves a single radar sensor, whereas multiple sensors could be as well co-deployed within the same physical space, giving rise to new opportunities and technical challenges to face, such as novel techniques to perform sensor fusion from multiple radar views, self-calibration algorithms for distributed radar sensors, as well as the transmission and compression of radar features from multiple sensing points. Other opportunities concern the combination of mmWave radar systems with camera-based ones (including thermal cameras), performing data/feature fusion across different sensing domains. Finally, a promising research avenue is to modify commercial off-the-shelf communication technology, such as the forthcoming IEEE 802.11ay, so as to exploit it as a passive mmWave radar. This would enable joint communications and passive sensing, without having to deploy a dedicated mmWave radar network.

As a general observation, the research on machine learning methods applied to device-based localization remains limited compared to device-free radar-based sensing. For device-based localization, machine learning methods find their typical application in fingerprinting approaches. Yet, these schemes require a typically lengthy preliminary measurement effort, which is often deemed excessive or impractical. Conversely, modern mmWave radar systems are both compact and affordable, and expose a number of features that can be more easily passed on to complex

learning and clustering algorithms to map environments, track movement, or estimate the occurrence of some events of interest. The applicability of machine learning algorithms to either field could change if more features become available, e.g., from multiple digital transceiver architectures integrated in the same client. For example, this would make it possible to use machine learning to increase the speed of intermediate localization algorithm steps (e.g., angle computations, ranging and simultaneous distance estimation among multiple mmWave devices, or joint angle/distance estimates based on radio features).

VIII. CONCLUSIONS

Millimeter-wave (mmWave) communication devices will soon become a fundamental component of 5G-and-beyond communication networks. This survey put the lens on recent research advances in localization and sensing algorithms for indoor mmWave communication and radar devices. After introducing the most important properties of mmWave signal propagation and communication chain architectures that enable mmWave channel measurements, we presented a thorough account of localization algorithms for mmWave devices. These are based on a broad range of techniques, that include both traditional methods based, e.g., on timing and received signal strength indicator (RSSI) information, and more specific methods that exploit the properties of mmWave devices and signal propagation, e.g., by processing channel state information (CSI).

Then, we turned our attention to consumer-grade mmWave radar devices, which are becoming extremely cost-effective sensing platforms. After introducing the basic structure of such radar architectures, we discussed different approaches that tackle applications such as human activity recognition, object detection and health monitoring. We unveiled that several research directions remain open in both fields, including better algorithms for localization and sensing with consumer-grade devices, data fusion methods for dense deployments, as well as an educated application of machine learning methods to both device-based localization and device-free sensing.

LIST OF ABBREVIATIONS

3GPP	Third-generation partnership project	LoS	line-of-sight
4G	fourth-generation	LSTM	long-short term memory
5G	fifth-generation		
A-BFT	association beamforming training	MAC	medium access control
ABT	asymmetric beamforming training	MCU	micro-controller unit
AD	angle-Doppler	MF	matched filter
ADC	analog-to-digital converter	MIMO	multiple-input multiple-output
ADoA	angle difference-of-arrival	MISO	multiple-input single-output
AE	autoencoder	ML	machine learning
AoA	angle of arrival	mmWave	millimeter-wave
AoD	angle of departure	MPC	multipath component
AP	access point	MUSIC	multiple signal classification
API	application program interfaces		
BI	beacon interval	NLoS	non line-of-sight
BRP	beam refinement protocol	NN	neural network
BS	base station		
CA-CFAR	cell-averaging constant false alarm rate	OKS	object keypoints similarity
CBAP	contention based access period		
CIR	channel impulse response	PA	power amplifier
CNN	convolutional NN	PDP	power-delay profile
COM	center of mass	PHY	physical layer
COTS	commercial off-the-shelf	PRS	positioning reference signal
CSI	channel state information	PSD	power spectral density
		PW	pulsed wave
DAC	digital-to-analog converter	RA	range-azimuth
DBSCAN	density-based spatial clustering of applications with noise	RD	range-Doppler
DFT	discrete Fourier transform	RDA	range-Doppler-azimuth
DKF	discrete KF	ResNet	residual network
DL	deep learning	RF	radio frequency
DSP	digital signal processor	RGB	red-green-blue
DTI	data transmission interval	RMS	root mean square
		RMSE	root mean square error
ECD	expand-contract dilation	RNN	recursive NN
EKF	extended Kalman filter	RSS	received signal strength
EM	expectation maximization	RSSI	received signal strength indicator
EN-DC	enhanced UTRA-dual connectivity	RTT	round-trip time
ESPRIT	estimation of signal parameters via rotational invariance techniques	RX	receive/receiver
		RZF	regularized zero-forcing
FCOS	fully connected one-stage	SAF	spatial attention fusion
FFT	fast Fourier transform	SAGE	space-alternating generalized expectation maximization
FMCW	frequency-modulated continuous wave	SDR	software-defined radio
FPGA	field-programmable gate array	SLAM	simultaneous localization and mapping
FSCN	fractionally strided convolutional network	SLS	sector-level sweep
FTM	fine time measurement	SNR	signal-to-noise ratio
		SoC	system-on-chip
GAN	generative adversarial network	SP	service period
GRU	gated recurrent unit	SPI	subsample peak interpolation
GSCM	geometry-based stochastic channel model	SRS	sounding reference signal
		SSW	sector sweep
HDC	hybrid dilated convolution	STA	station
HR	heart rate	STFT	short-time Fourier transform
HVRAE	hybrid variational RNN autoencoder	SV	Saleh-Valenzuela
		SVM	support vector machine
IF	intermediate-frequency	TDoA	time difference-of-arrival
IFFT	inverse FFT	ToA	time of arrival
IIR	infinite impulse response	ToF	time of flight
IoT	Internet of things	TX	transmit/transmitter
ITU-R	International telecommunication union – radiocommunication Sector	TXSS	transmit sweep
KF	Kalman filter	UAV	unmanned aerial vehicle
		UE	user equipment
LM	Levenberg-Marquardt	UKF	unscented Kalman filter
LMS	least mean squares	URLLC	ultra-reliable low-latency communications
		USRP	universal software radio peripheral
V2X	vehicle-to-everything		
VCO	voltage-controlled oscillator		
WLAN	wireless LAN		
ZF	zero-forcing		

REFERENCES

- [1] M. Xiao, S. Mumtaz, Y. Huang, L. Dai, Y. Li, M. Matthaiou, G. K. Karagiannidis, E. Björnson, K. Yang, I. Chih-Lin, and A. Ghosh, “Millimeter wave communications for future mobile networks (guest editorial), Part I,” *IEEE J. Sel. Areas Commun.*, vol. 35, no. 7, pp. 1425–1431, 2017.
- [2] X. Wang, L. Kong, F. Kong, F. Qiu, M. Xia, S. Arnon, and G. Chen, “Millimeter wave communication: A comprehensive survey,” *IEEE Commun. Surveys Tuts.*, vol. 20, no. 3, pp. 1616–1653, 2018.
- [3] A. N. Uwaechia and N. M. Mahyuddin, “A comprehensive survey on millimeter wave communications for fifth-generation wireless networks: Feasibility and challenges,” *IEEE Access*, vol. 8, pp. 62 367–62 414, 2020.
- [4] Z. Abu-Shaban, X. Zhou, T. Abhayapala, G. Seco-Granados, and H. Wymeersch, “Error bounds for uplink and downlink 3D localization in 5G millimeter wave systems,” *IEEE Trans. Wireless Commun.*, vol. 17, no. 8, pp. 4939–4954, 2018.
- [5] F. Ghasemimajm, Z. Abu-Shaban, S. S. Ikki, H. Wymeersch, and C. R. Benson, “Localization error bounds for 5G mmWave systems under I/Q imbalance,” *IEEE Trans. Veh. Technol.*, vol. 69, no. 7, pp. 7971–7975, 2020.
- [6] T. S. Rappaport, S. Sun, R. Mayzus, H. Zhao, Y. Azar, K. Wang, G. N. Wong, J. K. Schulz, M. Samimi, and F. Gutierrez, “Millimeter wave mobile communications for 5G cellular: It will work!” *IEEE Access*, vol. 1, pp. 335–349, 2013.
- [7] T. S. Rappaport, F. Gutierrez, E. Ben-Dor, J. N. Murdock, Y. Qiao, and J. I. Tamir, “Broadband millimeter-wave propagation measurements and models using adaptive-beam antennas for outdoor urban cellular communications,” *IEEE Trans. Antennas Propag.*, vol. 61, no. 4, pp. 1850–1859, Apr. 2013.
- [8] N. Peinecke, H. Doehler, and B. Korn, “Phong-like lighting for MMW radar simulation,” in *Proc. SPIE*, 8 2008, pp. 1–10.
- [9] L. Subrt, P. Pechac, and S. Zvanovec, “New approach to modeling of diffuse reflection and scattering for millimeter-wave systems in indoor scenarios,” *PIERS Online*, vol. 6, no. 8, pp. 719–722, 2010.
- [10] G. R. MacCartney, J. Zhang, S. Nie, and T. S. Rappaport, “Path loss models for 5G millimeter wave propagation channels in urban microcells,” in *Proc. IEEE GLOBECOM*, Dec. 2013, pp. 3948–3953.
- [11] M. Giordani, M. Mezzavilla, and M. Zorzi, “Initial access in 5G mmWave cellular networks,” *IEEE Commun. Mag.*, vol. 54, no. 11, pp. 40–47, Nov. 2016.
- [12] Y. Li, J. G. Andrews, F. Baccelli, T. D. Novlan, and J. C. Zhang, “Performance analysis of millimeter-wave cellular networks with two-stage beamforming initial access protocols,” in *Proc. Asilomar conf. on signals syst. and comput.*, Nov. 2016, pp. 1171–1175.
- [13] F. Devoti, I. Filippini, and A. Capone, “Facing the millimeter-wave cell discovery challenge in 5G networks with context-awareness,” *IEEE Access*, vol. 4, pp. 8019–8034, 2016.
- [14] T. Nitsche, C. Cordeiro, A. B. Flores, E. W. Knightly, E. Perahia, and J. C. Widmer, “IEEE 802.11ad: directional 60 GHz communication for multi-gigabit-per-second Wi-Fi,” *IEEE Commun. Mag.*, vol. 52, no. 12, pp. 132–141, 2014, invited paper.
- [15] IEEE, “IEEE Standard for Information technology—Telecommunications and information exchange between systems—Local and metropolitan area networks—Specific requirements—Part 11: Wireless LAN Medium Access Control (MAC) and Physical Layer (PHY) Specifications Amendment 3: Enhancements for Very High Throughput in the 60 GHz Band,” *Std 802.11ad-2012 (Amendment to IEEE Std 802.11-2012, as amended by IEEE Std 802.11ae-2012 and IEEE Std 802.11aa-2012)*, pp. 1–628, 2012.
- [16] P. Zhou, K. Cheng, X. Han, X. Fang, Y. Fang, R. He, Y. Long, and Y. Liu, “IEEE 802.11ay-based mmWave WLANs: Design challenges and solutions,” *IEEE Commun. Surveys Tuts.*, vol. 20, no. 3, pp. 1654–1681, 2018.
- [17] Y. Ghasempour, C. R. C. M. da Silva, C. Cordeiro, and E. W. Knightly, “IEEE 802.11ay: Next-generation 60 GHz communication for 100 Gb/s Wi-Fi,” *IEEE Commun. Mag.*, vol. 55, no. 12, pp. 186–192, 2017.
- [18] F. Zafari, A. Gkelias, and K. K. Leung, “A survey of indoor localization systems and technologies,” *IEEE Commun. Surveys Tuts.*, vol. 21, no. 3, pp. 2568–2599, 2019.
- [19] T. Kim Geok, K. Zar Aung, M. Sandar Aung, M. Thu Soe, A. Abdaziz, C. Pao Liew, F. Hossain, C. P. Tso, and W. H. Yong, “Review of indoor positioning: Radio wave technology,” *MDPI Applied Sciences*, vol. 11, no. 1, pp. 1–44, 2021.
- [20] K. Ngamakeur, S. Yongchareon, J. Yu, and S. U. Rehman, “A survey on device-free indoor localization and tracking in the multi-resident environment,” *ACM Comput. Surv.*, vol. 53, no. 4, pp. 1–29, Sep. 2020.
- [21] N. Singh, S. Choe, and R. Punmiya, “Machine learning based indoor localization using wi-fi rssi fingerprints: An overview,” *IEEE Access*, vol. 9, pp. 127 150–127 174, 2021.

[22] R. C. Shit, S. Sharma, D. Puthal, P. James, B. Pradhan, A. v. Moorsel, A. Y. Zomaya, and R. Ranjan, “Ubiquitous localization (UbiLoc): A survey and taxonomy on device free localization for smart world,” *IEEE Communications Surveys Tutorials*, vol. 21, no. 4, pp. 3532–3564, 2019.

[23] F. Wen, H. Wymeersch, B. Peng, W. P. Tay, H. C. So, and D. Yang, “A survey on 5G massive MIMO localization,” *Digital Signal Processing*, vol. 94, pp. 21–28, 2019.

[24] Z. Xiao and Y. Zeng, “An overview on integrated localization and communication towards 6G,” 2020, *arXiv preprint 2006.01535*, accessed: Sept. 2021. [Online]. Available: <https://arxiv.org/abs/2006.01535>

[25] C. De Lima, D. Belot, R. Berkvens, A. Bourdoux, D. Dardari, M. Guillaud, M. Isomursu, E.-S. Lohan, Y. Miao, A. N. Barreto, M. R. K. Aziz, J. Saloranta, T. Sanguanpuak, H. Sarieddeen, G. Seco-Granados, J. Suutala, T. Svensson, M. Valkama, B. Van Liempd, and H. Wymeersch, “Convergent communication, sensing and localization in 6G systems: An overview of technologies, opportunities and challenges,” *IEEE Access*, vol. 9, pp. 26 902–26 925, 2021.

[26] C. Laoudias, A. Moreira, S. Kim, S. Lee, L. Wirola, and C. Fischione, “A survey of enabling technologies for network localization, tracking, and navigation,” *IEEE Commun. Surveys Tuts.*, vol. 20, no. 4, pp. 3607–3644, 2018.

[27] J. Yang, J. Xu, X. Li, S. Jin, and B. Gao, “Integrated communication and localization in millimeter-wave systems,” *Frontiers of Information Tech. & Electronic Eng.*, vol. 22, no. 4, pp. 457–470, 2021.

[28] H. Tataria, K. Haneda, A. F. Molisch, M. Shafi, and F. Tufvesson, “Standardization of propagation models for terrestrial cellular systems: A historical perspective,” *International J. of Wireless Inf. Netw.*, vol. 28, pp. 20–44, Mar. 2021.

[29] M. Shafi, J. Zhang, H. Tataria, A. F. Molisch, S. Sun, T. S. Rappaport, F. Tufvesson, S. Wu, and K. Kitao, “Microwave vs. millimeter-wave propagation channels: Key differences and impact on 5G cellular systems,” *IEEE Commun. Mag.*, vol. 56, pp. 14–20, Dec. 2018.

[30] H. Tataria, S. Sangodoyin, A. F. Molisch, P. J. Smith, M. Matthaiou, J. Zhang, and R. S. Thomä, “Channel correlation diversity in mu-mimo systems—analysis and measurements,” in *2019 IEEE 30th Annual International Symposium on Personal, Indoor and Mobile Radio Communications (PIMRC)*. IEEE, 2019, pp. 1–7.

[31] P. B. Papazian, C. Gentile, K. A. Remley, J. Senic, and N. Golmie, “A radio channel sounder for mobile millimeter-wave communications: System implementation and measurement assessment,” *IEEE Trans. Microw. Theory Techn.*, vol. 64, pp. 2924–2932, Sep. 2016.

[32] J. Medbo, H. Asplund, J.-E. Berg, and N. Jalden, “Directional channel characteristics in elevation and azimuth at an urban macrocell base station,” in *Proc. EuCAP*, Mar. 2012, pp. 428–432.

[33] C. Gustafson, F. Tufvesson, S. Wyne, K. Haneda, and A. F. Molisch, “Directional analysis of measured 60 GHz indoor radio Channels using SAGE,” in *Proc. IEEE VTC-Spring*, Budapest, Hungary, May 2011, pp. 1–5.

[34] C. Schneider, M. Narandzic, M. Käské, G. Sommerkorn, and R. S. Thomä, “Large scale parameter for the WINNER II channel model at 2.53 GHz in urban macro cell,” in *Proc. IEEE VTC*, May 2010, pp. 1–5.

[35] G. R. Maccartney, T. S. Rappaport, S. Sun, and S. Deng, “Indoor Office Wideband Millimeter-Wave Propagation Measurements and Channel Models at 28 and 73 GHz for Ultra-Dense 5G Wireless Networks,” *IEEE Access*, vol. 3, pp. 2388–2424, 2015.

[36] W. Keusgen, R. J. Weiler, M. Peter, M. Wisotzki, and B. Göktepe, “Propagation measurements and simulations for millimeter-wave mobile access in a busy urban environment,” in *Proc. IRMMW-THz*, Sep. 2014, pp. 1–3.

[37] A. F. Molisch, *Wireless communications*. John Wiley & Sons, 2012, vol. 34.

[38] S. Jaeckel, L. Jiang, V. Jungnickel, L. Thiele, C. Jandura, G. Sommerkorn, and C. Schneider, “Correlation properties of large and small-scale parameters from multicell channel measurements,” in *Proc. EUCAP*, 2009, pp. 3406–3410.

[39] T. A. Thomas, H. C. Nguyen, G. R. MacCartney, and T. S. Rappaport, “3D mmWave Channel Model Proposal,” in *2014 IEEE 80th Vehicular Technology Conference (VTC2014-Fall)*, Sep. 2014, pp. 1–6.

[40] K. Haneda, N. Omaki, T. Imai, L. Raschkowski, M. Peter, and A. Roivainen, “Frequency-agile pathloss models for urban street canyons,” *IEEE Trans. Antennas Propag.*, vol. 64, pp. 1941–1951, May 2016.

[41] J. Ko, Y.-J. Cho, S. Hur, T. Kim, J. Park, A. F. Molisch, K. Haneda, M. Peter, D.-J. Park, and D.-H. Cho, “Millimeter-Wave Channel Measurements and Analysis for Statistical Spatial Channel Model in In-Building and Urban Environments at 28 GHz,” *IEEE Transactions on Wireless Communications*, vol. 16, pp. 5853–5868, Sep. 2017.

[42] H. J. Liebe, “An updated model for millimeter wave propagation in moist air,” *Radio Science*, vol. 20, pp. 1069–1089, Sep. 1985.

[43] S. Hur, S. Baek, B. Kim, Y. Chang, A. F. Molisch, T. S. Rappaport, K. Haneda, and J. Park, “Proposal on millimeter-wave channel modeling for 5g cellular system,” *IEEE J. Sel. Topics Signal Process.*, vol. 10, pp. 454–469, Apr. 2016.

[44] A. F. Molisch, A. Karttunen, S. Hur, J. Park, and J. Zhang, “Spatially consistent pathloss modeling for millimeter-wave channels in urban environments,” in *Proc. EuCAP*, Apr. 2016, pp. 1–5.

- [45] M. Steinbauer, A. Molisch, and E. Bonek, "The double-directional radio channel," *IEEE Antennas and Propagation Magazine*, vol. 43, pp. 51–63, Aug. 2001.
- [46] M.-D. Kim, J. Liang, J. Lee, J. Park, and B. Park, "Directional multipath propagation characteristics based on 28 GHz outdoor channel measurements," in *Proc. EuCAP*, Apr. 2016, pp. 1–5.
- [47] J. Poutanen, F. Tufvesson, K. Haneda, V.-M. Kolmonen, and P. Vainikainen, "Multi-link MIMO channel modeling using geometry-based approach," *IEEE Trans. Antennas Propag.*, vol. 60, pp. 587–596, Feb. 2012.
- [48] D. Dupleich, R. Müller, S. Skoblikov, C. Schneider, J. Luo, M. Boban, G. D. Galdo, and R. Thomä, "Multi-band Characterization of Path-loss, Delay, and Angular Spread in V2V Links," in *2018 IEEE 29th Annual International Symposium on Personal, Indoor and Mobile Radio Communications (PIMRC)*, Sep. 2018, pp. 85–90.
- [49] R. J. Weiler, M. Peter, W. Keusgen, K. Sakaguchi, and F. Undi, "Environment induced shadowing of urban millimeter-wave access links," *IEEE Wireless Commun. Lett.*, vol. 5, pp. 440–443, Aug. 2016.
- [50] H. C. Nguyen, I. Rodriguez, T. B. Sorensen, L. L. Sanchez, I. Kovacs, and P. Mogensen, "An empirical study of urban macro propagation at 10, 18 and 28 GHz," in *Proc. IEEE VTC-Spring*, May 2016, pp. 1–5.
- [51] S. Hur, Y.-J. Cho, T. Kim, J. Park, A. F. Molisch, K. Haneda, and M. Peter, "Wideband spatial channel model in an urban cellular environments at 28 GHz," in *Proc. EuCAP*, Apr. 2015, pp. 1–5.
- [52] A. Maltsev, A. Pudeyev, A. Lomayev, and I. Bolotin, "Channel modeling in the next generation mmWave Wi-Fi: IEEE 802.11ay standard," in *European Wireless 2016; 22th European Wireless Conference*, May 2016, pp. 1–8.
- [53] P. F. M. Smulders, "Statistical Characterization of 60-GHz Indoor Radio Channels," *IEEE Transactions on Antennas and Propagation*, vol. 57, pp. 2820–2829, Oct. 2009.
- [54] K. Haneda, J. Järveläinen, A. Karttunen, M. Kyrö, and J. Putkonen, "A Statistical Spatio-Temporal Radio Channel Model for Large Indoor Environments at 60 and 70 GHz," *IEEE Transactions on Antennas and Propagation*, vol. 63, pp. 2694–2704, Jun. 2015.
- [55] J. Kunisch and J. Pamp, "An ultra-wideband space-variant multipath indoor radio channel model," in *Proc. IEEE UWBST*, 2003, Nov. 2003, pp. 290–294.
- [56] W. Fu, J. Hu, and S. Zhang, "Frequency-domain measurement of 60 GHz indoor channels: a measurement setup, literature data, and analysis," *IEEE Instrumentation Measurement Magazine*, vol. 16, pp. 34–40, Apr. 2013.
- [57] L. Raschkowski, P. Kyösti, K. Kusume, and T. Jämsä, "METIS deliverable D1.4: Channel models," pp. 1–220, 2015, accessed: Sept. 2021. [Online]. Available: https://metis2020.com/wp-content/uploads/deliverables/METIS_D1.4_v1.0.pdf
- [58] G. R. MacCartney Jr., M. K. Samimi, and T. S. Rappaport, "Exploiting Directionality for Millimeter-Wave Wireless System Improvement," *arXiv:1503.05265 [cs, math]*, Mar. 2015, accessed: Sept. 2021.
- [59] Y. Xing, O. Kanhere, S. Ju, and T. S. Rappaport, "Indoor Wireless Channel Properties at Millimeter Wave and Sub-Terahertz Frequencies," in *2019 IEEE Global Communications Conference (GLOBECOM)*, Dec. 2019, pp. 1–6.
- [60] J. Medbo, H. Asplund, and J.-E. Berg, "60 GHz channel directional characterization using extreme size virtual antenna array," in *2015 IEEE 26th Annual International Symposium on Personal, Indoor, and Mobile Radio Communications (PIMRC)*, Aug. 2015, pp. 176–180.
- [61] M. Shafi, A. F. Molisch, P. J. Smith, T. Haustein, P. Zhu, P. D. Silva, F. Tufvesson, A. Benjebbour, and G. Wunder, "5G: A tutorial overview of standards, trials, challenges, deployment, and practice," *IEEE J. Sel. Areas Commun.*, vol. 35, pp. 1201–1221, Jun. 2017.
- [62] 3GPP, "Study on channel model for frequencies from 0.5 to 100 GHz," *3rd Generation Partnership Project (3GPP), Tech. Rep. 38.901*, vol. 38, 2018.
- [63] M. Series, "Guidelines for evaluation of radio interface technologies for imt-2020," *Report ITU*, pp. 2412–0, 2017.
- [64] J. Poutanen, K. Haneda, L. Liu, C. Oestges, F. Tufvesson, and P. Vainikainen, "Parameterization of the COST 2100 MIMO channel model in indoor scenarios," in *Proc. EUCAP*, 2011, pp. 3606–3610.
- [65] S. Jaeckel, L. Raschkowski, K. Börner, L. Thiele, F. Burkhardt, and E. Eberlein, "Quadriga-quasi deterministic radio channel generator, user manual and documentation," *Fraunhofer Heinrich Hertz Institute, Tech. Rep. v2. 4.0*, 2020.
- [66] S. Ju, Y. Xing, O. Kanhere, and T. S. Rappaport, "3-d statistical indoor channel model for millimeter-wave and sub-terahertz bands," in *GLOBECOM 2020-2020 IEEE Global Communications Conference*. IEEE, 2020, pp. 1–7.
- [67] S. Hur, H. Yu, J. Park, W. Roh, C. U. Bas, R. Wang, and A. F. Molisch, "Feasibility of mobility for millimeter-wave systems based on channel measurements," *IEEE Commun. Mag.*, vol. 56, pp. 56–63, Jul. 2018.
- [68] H. Tataria and F. Tufvesson, "Impact of spatially consistent channels on digital beamforming for millimeter-wave systems," in *Proc. EuCAP*, Mar. 2020, pp. 1–5.

[69] R. J. Weiler, M. Peter, W. Keusgen, A. Maltsev, I. Karls, A. Pudeyev, I. Bolotin, I. Siaud, and A.-M. Ulmer-Moll, “Quasi-deterministic millimeter-wave channel models in miweba,” *EURASIP J. on Wireless Commun. and Networking*, vol. 2016, p. 84, Mar. 2016.

[70] L. Liu, C. Oestges, J. Poutanen, K. Haneda, P. Vainikainen, F. Qutin, F. Tufvesson, and P. D. Doncker, “The COST 2100 MIMO channel model,” *IEEE Wireless Communications*, vol. 19, pp. 92–99, Dec. 2012.

[71] K. Haneda *et al.*, “5G 3GPP-like channel models for outdoor urban microcellular and macrocellular environments,” in *Proc. IEEE VTC-Spring*, May 2016, pp. 1–7.

[72] S. Ju, Y. Xing, O. Kanhere, and T. S. Rappaport, “Millimeter wave and sub-terahertz spatial statistical channel model for an indoor office building,” *IEEE Journal on Selected Areas in Communications*, vol. 39, no. 6, pp. 1561–1575, 2021.

[73] F. Khan and Z. Pi, “mmWave mobile broadband (MMB): Unleashing the 3–300 GHz spectrum,” in *Proc. IEEE Sarnoff Symposium*, May 2011, pp. 1–6.

[74] W. Roh, J.-Y. Seol, J. Park, B. Lee, J. Lee, Y. Kim, J. Cho, K. Cheun, and F. Aryanfar, “Millimeter-wave beamforming as an enabling technology for 5G cellular communications: theoretical feasibility and prototype results,” *IEEE Commun. Mag.*, vol. 52, pp. 106–113, Feb. 2014.

[75] A. F. Molisch, V. V. Ratnam, S. Han, Z. Li, S. L. H. Nguyen, L. Li, and K. Haneda, “Hybrid beamforming for massive MIMO: A survey,” *IEEE Commun. Mag.*, vol. 55, pp. 134–141, Sep. 2017.

[76] O. E. Ayach, R. W. Heath, S. Abu-Surra, S. Rajagopal, and Z. Pi, “Low complexity precoding for large millimeter wave MIMO systems,” in *Proc. IEEE ICC*, Jun. 2012, pp. 3724–3729.

[77] T. Kim, J. Park, J.-Y. Seol, S. Jeong, J. Cho, and W. Roh, “Tens of Gbps support with mmWave beamforming systems for next generation communications,” in *Proc. IEEE GLOBECOM*, Dec. 2013, pp. 3685–3690.

[78] J. Song, J. Choi, and D. J. Love, “Codebook design for hybrid beamforming in millimeter wave systems,” in *Proc. IEEE ICC*, Jun. 2015, pp. 1298–1303.

[79] S. Payami, M. Shariat, M. Ghoraishi, and M. Dianati, “Effective RF codebook design and channel estimation for millimeter wave communication systems,” in *Proc. IEEE ICCW*, Jun. 2015, pp. 1226–1231.

[80] S. Dutta, C. N. Barati, D. Ramirez, A. Dhananjay, J. F. Buckwalter, and S. Rangan, “A case for digital beamforming at mmWave,” *IEEE Trans. Wireless Commun.*, vol. 19, pp. 756–770, Feb. 2020.

[81] B. Yang, Z. Yu, J. Lan, R. Zhang, J. Zhou, and W. Hong, “Digital beamforming-based massive MIMO transceiver for 5G millimeter-wave communications,” *IEEE Trans. Microw. Theory Techn.*, vol. 66, pp. 3403–3418, Jul. 2018.

[82] Y. Hu, “A digital multibeam array with wide scanning angle and enhanced beam gain for millimeter-wave massive MIMO applications,” *IEEE Trans. Antennas Propag.*, vol. 66, p. 11, 2018.

[83] P. Xingdong, H. Wei, Y. Tianyang, and L. Linsheng, “Design and implementation of an active multibeam antenna system with 64 RF channels and 256 antenna elements for massive MIMO application in 5G wireless communications,” *China Communications*, vol. 11, pp. 16–23, Nov. 2014.

[84] C. Yu, J. Jing, H. Shao, Z. H. Jiang, P. Yan, X.-W. Zhu, W. Hong, and A. Zhu, “Full-angle digital predistortion of 5G millimeter-wave massive MIMO transmitters,” *IEEE Trans. Microw. Theory Techn.*, vol. 67, pp. 2847–2860, Jul. 2019.

[85] 3GPP, “Study on nr positioning enhancements,” *3rd Generation Partnership Project (3GPP), Tech. Rep.*, vol. 38.857, March 2021.

[86] X. Li, E. Leitinger, M. Oskarsson, K. Astrom, and F. Tufvesson, “Massive MIMO-based localization and mapping exploiting phase information of multipath components,” *IEEE Trans. Wireless Commun.*, vol. 18, pp. 4254–4267, Sep. 2019.

[87] J. Palacios, D. Steinmetzer, A. Loch, M. Hollick, and J. Widmer, “Adaptive codebook optimization for beam training on off-the-shelf IEEE 802.11ad devices,” in *Proc. ACM MobiCom*, Oct. 2018, p. 241–255.

[88] Y. Xie, J. Xiong, M. Li, and K. Jamieson, “MD-Track: Leveraging multi-dimensionality for passive indoor Wi-Fi tracking,” in *Proc. ACM MobiCom*, Aug. 2019, pp. 1–16.

[89] R. Schmidt, “Multiple emitter location and signal parameter estimation,” *IEEE Trans. Antennas Propag.*, vol. 34, no. 3, pp. 276–280, 1986.

[90] A. Paulraj, R. Roy, and T. Kailath, “Estimation of signal parameters via rotational invariance techniques – ESPRIT,” in *Proc. Asilomar conf. on signals syst. and comput.*, 1985, pp. 83–89.

[91] “Talon AD7200,” 2020, accessed: Sept. 2021. [Online]. Available: <https://www.tp-link.com/us/home-networking/wifi-router/ad7200/>

[92] J. Palacios, G. Bielsa, P. Casari, and J. Widmer, “Communication-driven localization and mapping for millimeter wave networks,” in *Proc. IEEE INFOCOM*, 2018, pp. 2402–2410.

[93] M. Petri and M. Ehrig, "A SoC-based SDR platform for ultra-high data rate broadband communication, radar and localization systems," in *Proc. Wireless Days*, 2019, pp. 1–4.

[94] N. Maletic, V. Sark, M. Ehrig, J. Gutiérrez, and E. Grass, "Experimental evaluation of round-trip tof-based localization in the 60 ghz band," in *Proc. IPIN*, 2019, pp. 1–6.

[95] S. Saha, Y. Ghasempour, M. Haider, T. Siddiqui, P. Melo, N. Somanchi, L. Zakrajsek, A. Singh, R. Shyamsunder, O. Torres, D. Uvaydov, J. Jornet, E. Knightly, D. Koutsonikolas, D. Pados, Z. Sun, and N. Thawdar, "X60: A programmable testbed for wideband 60 GHz WLANs with phased arrays," *Computer Communications*, vol. 133, 09 2018.

[96] S. Aggarwal, U. S. Sardesai, V. Sinha, and D. Koutsonikolas, "An experimental study of rate and beam adaptation in 60 GHz WLANs," in *Proc. ACM MSWiM*, 2020, p. 171–180.

[97] J. Zhang, X. Zhang, P. Kulkarni, and P. Ramanathan, "OpenMili: a 60 GHz software radio platform with a reconfigurable phased-array antenna," 2016, pp. 162–175.

[98] "Pi-radio," 2020, accessed: Sept. 2021. [Online]. Available: <https://www.pi-rad.io>

[99] "Zync ZCU111," 2020, accessed: July 2021. [Online]. Available: <https://www.xilinx.com/products/boards-and-kits/zcu111.html>

[100] I. Pefkianakis and K.-H. Kim, "Accurate 3D localization for 60 GHz networks," in *Proc. ACM SenSys*, 2018, p. 120–131.

[101] G. Bielsa, J. Palacios, A. Loch, D. Steinmetzer, P. Casari, and J. Widmer, "Indoor localization using commercial off-the-shelf 60 GHz access points," in *Proc. IEEE INFOCOM*, 2018, pp. 2384–2392.

[102] A. Olivier, G. Bielsa, I. Tejado, M. Zorzi, J. Widmer, and P. Casari, "Lightweight indoor localization for 60-GHz millimeter wave systems," in *Proc. IEEE SECON*, 2016, pp. 1–9.

[103] J. Palacios, G. Bielsa, P. Casari, and J. Widmer, "Single-and multiple-access point indoor localization for millimeter-wave networks," *IEEE Trans. Wireless Commun.*, vol. 18, no. 3, pp. 1927–1942, 2019.

[104] J. Palacios, P. Casari, H. Assasa, and J. Widmer, "LEAP: Location estimation and predictive handover with consumer-grade mmWave devices," in *Proc. IEEE INFOCOM*, 2019, pp. 2377–2385.

[105] M. Pajovic, P. Wang, T. Koike-Akino, H. Sun, and P. V. Orlik, "Fingerprinting-based indoor localization with commercial mmWave WiFi - part I: RSS and beam indices," in *Proc. IEEE GLOBECOM*, 2019, pp. 1–6.

[106] A. Vashist, D. R. Bhanushali, R. Relyea, C. Hochgraf, A. Ganguly, P. D. Sai Manoj, R. Ptucha, A. Kwasinski, and M. E. Kuhl, "Indoor wireless localization using consumer-grade 60 GHz equipment with machine learning for intelligent material handling," in *Proc. IEEE ICCE*, 2020, pp. 1–6.

[107] P. Wang, M. Pajovic, T. Koike-Akino, H. Sun, and P. V. Orlik, "Fingerprinting-based indoor localization with commercial mmWave WiFi - Part II: Spatial beam SNRs," in *Proc. IEEE GLOBECOM*, 2019, pp. 1–6.

[108] T. Koike-Akino, P. Wang, M. Pajovic, H. Sun, and P. V. Orlik, "Fingerprinting-based indoor localization with commercial MMWave WiFi: A deep learning approach," *IEEE Access*, vol. 8, pp. 84 879–84 892, 2020.

[109] P. Wang, T. Koike-Akino, and P. V. Orlik, "Fingerprinting-based indoor localization with commercial mmWave WiFi: NLOS propagation," in *Proc. IEEE GLOBECOM*, 2020, pp. 1–6.

[110] A. Zhou, S. Yang, Y. Yang, Y. Fan, and H. Ma, "Autonomous environment mapping using commodity millimeter-wave network device," in *Proc. IEEE INFOCOM*, 2019, pp. 1126–1134.

[111] O. Kanhere, S. Ju, Y. Xing, and T. S. Rappaport, "Map-assisted millimeter wave localization for accurate position location," in *Proc. IEEE GLOBECOM*, 2019, pp. 1–6.

[112] N. Maletic, V. Sark, J. Gutiérrez, and E. Grass, "Device localization using mmWave ranging with sub-6-assisted angle of arrival estimation," in *Proc. IEEE BMSB*, 2018, pp. 1–6.

[113] D. Garcia, J. O. Lacruz, P. Jiménez Mateo, and J. Widmer, "POLAR: Passive object localization with IEEE 802.11ad using phased antenna arrays," in *Proc. IEEE INFOCOM*, 2020, pp. 1838–1847.

[114] S. Wang, J. Huang, X. Zhang, H. Kim, and S. Dey, "X-Array: approximating omnidirectional millimeter-wave coverage using an array of phased arrays," in *Proc. ACM MobiCom*, 2020, pp. 1–14.

[115] "Airfide Inc." 2019, accessed: June 2021. [Online]. Available: <http://airfidenet.com>

[116] D. Steinmetzer, D. Wegemer, M. Schulz, J. Widmer, and M. Hollick, "Compressive millimeter-wave sector selection in off-the-shelf IEEE 802.11ad devices," in *Proc. ACM CoNEXT*, 2017.

[117] C. R. C. M. Da Silva, J. Kosloff, C. Chen, A. Lomayev, and C. Cordeiro, "Beamforming training for IEEE 802.11ay millimeter wave systems," in *Proc. IEEE ITA*, 2018, pp. 1–9.

- [118] F. Gu, X. Hu, M. Ramezani, D. Acharya, K. Khoshelham, S. Valaee, and J. Shang, “Indoor localization improved by spatial context—a survey,” *ACM Comput. Surv.*, vol. 52, no. 3, pp. 1–35, Jul. 2019.
- [119] A. Yassin, Y. Nasser, M. Awad, and A. Al-Dubai, “Simultaneous context inference and mapping using mm-Wave for indoor scenarios,” in *Proc. IEEE ICC*, 2017, pp. 1–6.
- [120] J. Palacios, P. Casari, and J. Widmer, “JADE: Zero-knowledge device localization and environment mapping for millimeter wave systems,” in *Proc. IEEE INFOCOM*, 2017, pp. 1–9.
- [121] A. Fascista, A. Coluccia, H. Wymeersch, and G. Seco-Granados, “Low-complexity accurate mmwave positioning for single-antenna users based on angle-of-departure and adaptive beamforming,” in *Proc. IEEE ICASSP*, 2020, pp. 4866–4870.
- [122] Y. Lin, S. Jin, M. Matthaiou, and X. You, “Channel estimation and indoor positioning for wideband multiuser millimeter wave systems,” in *Proc. IEEE SAM*, 2020, pp. 1–5.
- [123] H. Ajorloo, C. J. Sreenan, A. Loch, and J. Widmer, “On the feasibility of using IEEE 802.11ad mmWave for accurate object detection,” in *Proc. ACM/SIGAPP SAC*, 2019, p. 2406–2413.
- [124] M. Vari and D. Cassioli, “mmWaves RSSI indoor network localization,” in *Proc. IEEE ICC*, 2014, pp. 127–132.
- [125] K. He, X. Zhang, S. Ren, and J. Sun, “Deep residual learning for image recognition,” in *Proc. IEEE CVPR*, 2016, pp. 770–778.
- [126] Z. Lin, T. Lv, and P. T. Mathiopoulos, “3-D indoor positioning for millimeter-wave massive MIMO systems,” *IEEE Trans. Commun.*, vol. 66, no. 6, pp. 2472–2486, Jun. 2018.
- [127] Z. Wei, Y. Zhao, X. Liu, and Z. Feng, “DoA-LF: A location fingerprint positioning algorithm with millimeter-wave,” *IEEE Access*, vol. 5, pp. 22 678–22 688, 2017.
- [128] P. Hong, C. Li, H. Chang, Y. Hsueh, and K. Wang, “WBF-PS: WiGig beam fingerprinting for UAV positioning system in GPS-denied environments,” in *Proc. IEEE INFOCOM*, 2020, pp. 1778–1787.
- [129] T. T. Tsai, L. H. Shen, C. J. Chiu, and K. T. Feng, “Beam AoD-based Indoor Positioning for 60 GHz mmWave System,” in *Proc. IEEE VTC-Fall*, 2020, pp. 1–5.
- [130] J. Chen, D. Steinmetzer, J. Classen, E. Knightly, and M. Hollick, “Pseudo lateration: Millimeter-wave localization using a single RF chain,” in *Proc. IEEE WCNC*, 2017, pp. 1–6.
- [131] Y. Jia, H. Tian, S. Fan, and B. Liu, “Motion feature and millimeter wave multi-path AoA-ToA based 3D indoor positioning,” in *Proc. IEEE PIMRC*, 2018, pp. 1–7.
- [132] B. Hu, H. Tian, and S. Fan, “Millimeter wave LOS/NLOS identification and localization via mean-shift clustering,” in *Proc. IEEE PIMRC*, 2019, pp. 1–7.
- [133] F. Fellhauer, J. Lassen, A. Jaber, N. Loghin, and S. Ten Brink, “Non-line-of-sight positioning for mmwave communications,” in *Proc. IEEE SPAWC*, 2018, pp. 1–5.
- [134] A. Yassin, Y. Nasser, and M. Awad, “Geometric approach in simultaneous context inference, localization and mapping using mm-Wave,” in *Proc. ICT*, 2018, pp. 159–164.
- [135] A. Yassin, Y. Nasser, A. Y. Al-Dubai, and M. Awad, “MOSAIC: Simultaneous localization and environment mapping using mmWave without a-priori knowledge,” *IEEE Access*, vol. 6, pp. 68 932–68 947, 2018.
- [136] O. AlHory, O. Shoushara, H. AlSuri, M. ALShunnaq, and F. Awad, “5G mmWave indoor location identification using beamforming and RSSI,” in *Proc. ICICS*, 2020, pp. 91–95.
- [137] M. Z. Comiter, M. B. Crouse, and H. T. Kung, “A data-driven approach to localization for high frequency wireless mobile networks,” in *Proc. IEEE GLOBECOM*, 2017, pp. 1–7.
- [138] A. Yassin, Y. Nasser, Y. Corre, G. Gougeon, and Y. Lostanlen, “3D localization and mapping using mm-Wave: What are the opportunities in vehicular and indoor environments?” in *Proc. ICT*, 2018, pp. 324–330.
- [139] A. Davoli, G. Guerzoni, and G. M. Vitetta, “Machine learning and deep learning techniques for colocated MIMO radars: A tutorial overview,” *IEEE Access*, vol. 9, pp. 33 704–33 755, 2021.
- [140] B. van Berlo, A. Elkelany, T. Ozcelebi, and N. Meratnia, “Millimeter wave sensing: A review of application pipelines and building blocks,” *IEEE Sensors J.*, vol. 21, no. 9, pp. 10 332–10 368, 2021.
- [141] M. Jankiraman, *FMCW Radar Design*. Artech House, 2018.
- [142] C. Iovescu and S. Rao, “The fundamentals of millimeter wave sensors,” Texas Instruments, Tech. Rep. SPYY005A, 2017.
- [143] A. E. Omer, S. Safavi-Naeini, R. Hughson, and G. Shaker, “Blood glucose level monitoring using an FMCW millimeter-wave radar sensor,” *Remote Sensing*, vol. 12, no. 3, pp. 1–25, 2020.

- [144] A. E. Omer, G. Shaker, S. Safavi-Naeini, K. Murray, and R. Hughson, "Glucose levels detection using mm-wave radar," *IEEE Sensors lett.*, vol. 2, no. 3, pp. 1–4, 2018.
- [145] J. Pegoraro, F. Meneghelli, and M. Rossi, "Multiperson continuous tracking and identification from mm-Wave micro-doppler signatures," *IEEE Trans. Geosci. Remote Sens.*, vol. 59, no. 4, pp. 2994–3009, 2021.
- [146] T. Gu, Z. Fang, Z. Yang, P. Hu, and P. Mohapatra, "Mmsense: Multi-person detection and identification via mmwave sensing," in *Proc. ACM mmNets*, 2019, pp. 45–50.
- [147] Z. Yang, P. H. Pathak, Y. Zeng, X. Liran, and P. Mohapatra, "Vital sign and sleep monitoring using millimeter wave," *ACM Trans. on Sensor Networks*, vol. 13, no. 2, pp. 1–32, 2017.
- [148] S. D. Regani, C. Wu, B. Wang, M. Wu, and K. J. R. Liu, "mmWrite: Passive handwriting tracking using a single millimeter wave radio," *IEEE Internet Things J.*, pp. 1–1, 2021, in press.
- [149] M. Alizadeh, G. Shaker, and S. Safavi-Naeini, "Remote health monitoring system for bedbound patients," in *Proc. IEEE BIBE*, 2020, pp. 801–806.
- [150] C. X. Lu, S. Rosa, P. Zhao, B. Wang, C. Chen, J. A. Stankovic, N. Trigoni, and A. Markham, "See through smoke: robust indoor mapping with low-cost mmWave radar," in *Proc. ACM MobiSys*, 2020, pp. 14–27.
- [151] M. Z. Ozturk, C. Wu, B. Wang, and K. J. R. Liu, "GaitCube: Deep data cube learning for human recognition with millimeter-wave radio," *IEEE Internet Things J.*, 2021, in press.
- [152] H. Cui and N. Dahnoun, "High precision human detection and tracking using millimeter-wave radars," *IEEE Aerosp. Electron. Syst. Mag.*, vol. 36, pp. 22–32, 2021.
- [153] Y. Wang, H. Liu, K. Cui, A. Zhou, W. Li, and H. Ma, "m-Activity: Accurate and real-time human activity recognition via millimeter wave radar," in *Proc. IEEE ICASSP*, 2021, pp. 8298–8302.
- [154] J. W. Smith, S. Thiagarajan, R. Willis, Y. Makris, and M. Torlak, "Improved static hand gesture classification on deep convolutional neural networks using novel sterile training technique," *IEEE Access*, vol. 9, pp. 10 893–10 902, 2021.
- [155] R. Zhang and S. Cao, "Real-time human motion behavior detection via CNN using mmWave radar," *IEEE Sensors J.*, vol. 3, no. 2, pp. 1–4, 2018.
- [156] G. Tiwari and S. Gupta, "An mmWave radar based real-time contactless fitness tracker using deep CNNs," *IEEE Sensors J.*, vol. 21, no. 15, pp. 17 262–17 270, 2021.
- [157] F. Jin, R. Zhang, A. Sengupta, S. Cao, S. Hariri, N. K. Agarwal, and S. K. Agarwal, "Multiple patients behavior detection in real-time using mmWave radar and deep CNNs," in *Proc. IEEE RadarConf.* IEEE, 2019, pp. 1–6.
- [158] A. Sengupta, F. Jin, R. Zhang, and S. Cao, "Mm-pose: Real-time human skeletal posture estimation using mmWave radars and CNNs," *IEEE Sensors J.*, vol. 20, no. 17, pp. 10 032–10 044, 2020.
- [159] C. Jiang, J. Guo, Y. He, M. Jin, S. Li, and Y. Liu, "Mmvib: Micrometer-level vibration measurement with mmwave radar," in *Proc. ACM MobiCom*, 2020, pp. 1–13.
- [160] D. F. Albuquerque, E. S. Goncalves, E. F. Pedrosa, F. C. Teixeira, and J. N. Vieira, "Robot self position based on asynchronous millimetre wave radar interference," in *Proc. IPIN*, 2019.
- [161] G. Li, Z. Zhang, H. Yang, J. Pan, D. Chen, and J. Zhang, "Capturing human pose using mmWave radar," in *Proc. IEEE PerCom Workshops*. IEEE, 2020, pp. 1–6.
- [162] F. Jin, A. Sengupta, and S. Cao, "mmFall: Fall detection using 4-D mmWave radar and a hybrid variational RNN autoencoder," *IEEE Trans. Autom. Sci. Eng.*, pp. 1–13, 2020, in press.
- [163] T. K. Vodai, K. Oleksak, T. Kvelashvili, F. Foroughian, C. Bauder, P. Theilmann, A. Fathy, and O. Kilic, "Enhancement of remote vital sign monitoring detection accuracy using multiple-input multiple-output 77 GHz FMCW radar," *IEEE Journal of Electromagnetics, RF and Microwaves in Medicine and Biology*, pp. 1–1, 2021, in press.
- [164] P. Zhao, C. X. Lu, B. Wang, C. Chen, L. Xie, M. Wang, N. Trigoni, and A. Markham, "Heart rate sensing with a robot mounted mmwave radar," in *Proc. IEEE ICRA*. IEEE, 2020, pp. 2812–2818.
- [165] D. Nickalls, J. Wu, and N. Dahnoun, "A real-time and high performance posture estimation system based on millimeter-wave radar," in *Proc. MECO*, 2021, pp. 1–4.
- [166] H. Cui and N. Dahnoun, "High precision human detection and tracking using millimeter-wave radars," *IEEE Aerosp. Electron. Syst. Mag.*, vol. 36, no. 1, pp. 22–32, 2021.
- [167] J. Wu, H. Cui, and N. Dahnoun, "A novel high performance human detection, tracking and alarm system based on millimeter-wave radar," in *Proc. MECO*, 2021, pp. 1–4.

[168] V. C. Chen, F. Li, S.-S. Ho, and H. Wechsler, "Micro-doppler effect in radar: phenomenon, model, and simulation study," *IEEE Trans. Aerosp. Electron. Syst.*, vol. 42, no. 1, pp. 2–21, 2006.

[169] J. B. Allen and L. R. Rabiner, "A unified approach to short-time fourier analysis and synthesis," *Proc. IEEE*, vol. 65, no. 11, pp. 1558–1564, 1977.

[170] L. Cohen, *Time-frequency analysis*. Prentice Hall, 1995, vol. 778.

[171] V. Chen, D. Tahmoush, and W. Miceli, *Radar Micro-Doppler Signatures: Processing and Applications*. IET, 2014.

[172] R. E. Kalman, "A New Approach to Linear Filtering and Prediction Problems," *J. Basic Eng.*, vol. 82, no. 1, pp. 35–45, 1960.

[173] G. Welch, G. Bishop *et al.*, "An introduction to the kalman filter," University of North Carolina at Chapel Hill, Dept. of Computer Science, Tech. Rep. TR 95-041, 1995, accessed: Sept. 2021. [Online]. Available: https://www.cs.unc.edu/~welch/media/pdf/kalman_intro.pdf

[174] S. J. Julier and J. K. Uhlmann, "Reduced sigma point filters for the propagation of means and covariances through nonlinear transformations," in *Proc. IEEE ACC*, vol. 2. IEEE, 2002, pp. 887–892.

[175] E. A. Wan and R. Van Der Merwe, "The unscented Kalman filter for nonlinear estimation," in *Proc. IEEE AS-SPCC*. IEEE, 2000, pp. 153–158.

[176] J. Pegoraro and M. Rossi, "Real-time people tracking and identification from sparse mm-wave radar point-clouds," *IEEE Access*, vol. 9, pp. 78 504–78 520, 2021.

[177] T. M. Mitchell *et al.*, "Machine learning," 1997.

[178] I. Goodfellow, Y. Bengio, A. Courville, and Y. Bengio, *Deep learning*. MIT press Cambridge, 2016, vol. 1, no. 2.

[179] M. Ester, H.-P. Kriegel, J. Sander, X. Xu *et al.*, "A density-based algorithm for discovering clusters in large spatial databases with noise," in *Proc. AAAI KDD*, vol. 96, no. 34, 1996, pp. 226–231.

[180] V. Estivill-Castro, "Why so many clustering algorithms: a position paper," *ACM SIGKDD explorations newsletter*, vol. 4, no. 1, pp. 65–75, 2002.

[181] D. Kellner, J. Klappstein, and K. Dietmayer, "Grid-based DBSCAN for clustering extended objects in radar data," in *Proc. IEEE IVS*. IEEE, 2012, pp. 365–370.

[182] U. Hasson, S. A. Nastase, and A. Goldstein, "Direct fit to nature: An evolutionary perspective on biological and artificial neural networks," *Neuron*, vol. 105, no. 3, pp. 416–434, 2020.

[183] F. Rosenblatt, "The perceptron: a probabilistic model for information storage and organization in the brain." *Psychological review*, vol. 65, no. 6, p. 386, 1958.

[184] Y. LeCun, L. Bottou, Y. Bengio, and P. Haffner, "Gradient-based learning applied to document recognition," *Proc. IEEE*, vol. 86, no. 11, pp. 2278–2324, 1998.

[185] S. Chang, Y. Zhang, F. Zhang, X. Zhao, S. Huang, Z. Feng, and Z. Wei, "Spatial attention fusion for obstacle detection using mmwave radar and vision sensor," *Sensors*, vol. 20, no. 4, pp. 1–21, 2020.

[186] R. J. Williams and J. Peng, "An efficient gradient-based algorithm for on-line training of recurrent network trajectories," *Neural computation*, vol. 2, no. 4, pp. 490–501, 1990.

[187] S. Hochreiter and J. Schmidhuber, "Long short-term memory," *Neural computation*, vol. 9, no. 8, pp. 1735–1780, 1997.

[188] S. Hochreiter, "The vanishing gradient problem during learning recurrent neural nets and problem solutions," *International Journal of Uncertainty, Fuzziness and Knowledge-Based Systems*, vol. 6, no. 02, pp. 107–116, 1998.

[189] P. Zhao, C. X. Lu, J. Wang, C. Chen, W. Wang, N. Trigoni, and A. Markham, "mID: Tracking and identifying people with millimeter wave radar," in *Proc. DCOSS*, 2019, pp. 33–40.

[190] P. Vincent, H. Larochelle, I. Lajoie, Y. Bengio, and P.-A. Manzagol, "Stacked denoising autoencoders: Learning useful representations in a deep network with a local denoising criterion," *J. Mach. Learn. Res.*, vol. 11, p. 3371–3408, 2010.

[191] S. Wagner and W. Johann, "Target detection using autoencoders in a radar surveillance system," in *Proc. IEEE RadarConf*. IEEE, 2019, pp. 1–5.

[192] I. Goodfellow, J. Pouget-Abadie, M. Mirza, B. Xu, D. Warde-Farley, S. Ozair, A. Courville, and Y. Bengio, "Generative adversarial networks," *Commun. ACM*, vol. 63, no. 11, p. 139–144, Oct. 2020.

[193] S. Ioffe and C. Szegedy, "Batch normalization: Accelerating deep network training by reducing internal covariate shift," in *Proc. ICML*, 2015, pp. 448–456.

[194] C. R. Qi, H. Su, K. Mo, and L. J. Guibas, "Pointnet: Deep learning on point sets for 3D classification and segmentation," in *Proc. IEEE CVPR*, 2017, pp. 652–660.

- [195] C. R. Qi, L. Yi, H. Su, and L. J. Guibas, “Pointnet++: Deep hierarchical feature learning on point sets in a metric space,” 2017, arXiv preprint 1706.02413.
- [196] W. Wu, Z. Qi, and L. Fuxin, “PointConv: Deep convolutional networks on 3D point clouds,” in *Proc. IEEE CVPR*, 2019, pp. 9613–9622.
- [197] Z. Meng, S. Fu, J. Yan, H. Liang, A. Zhou, S. Zhu, H. Ma, J. Liu, and N. Yang, “Gait recognition for co-existing multiple people using millimeter wave sensing,” in *Proc. AAAI Conf. on Artificial Intelligence*, 2020, pp. 849–856.
- [198] D.-S. Lee, S. Yeom, J.-Y. Son, and S.-H. Kim, “Automatic image segmentation for concealed object detection using the expectation–maximization algorithm,” *Optics express*, vol. 18, no. 10, pp. 10 659–10 667, 2010.
- [199] S. Yeom, D.-S. Lee, J.-Y. Son, M.-K. Jung, Y. Jang, S.-W. Jung, and S.-J. Lee, “Real-time outdoor concealed-object detection with passive millimeter wave imaging,” *Optics express*, vol. 19, no. 3, pp. 2530–2536, 2011.
- [200] T. Wei and X. Zhang, “Mtrack: High-precision passive tracking using millimeter wave radios,” in *Proc. ACM MobiCom*, 2015, p. 117–129.
- [201] B. Kapilevich, Y. Pinhasi, M. Anisimov, B. Litvak, and D. Hardon, “FMCW mm-wave non-imaging sensor for detecting hidden objects,” in *Proc. IEEE MTT-S IMWS*, 2011, pp. 101–104.
- [202] B. Kapilevich, B. Litvak, and A. Shulzinger, “Passive non-imaging mm-wave sensor for detecting hidden objects,” in *Proc. IEEE COMCAS*, 2013, pp. 1–5.
- [203] J. Bhatia, A. Dayal, A. Jha, S. K. Vishvakarma, J. Soumya, M. B. Srinivas, P. K. Yalavarthy, A. Kumar, V. Lalitha, S. Koorapati, and L. R. Cenkeramaddi, “Object classification technique for mmWave FMCW radars using range-FFT features,” in *Proc. COMSNETS*, 2021, pp. 111–115.
- [204] C. Wang, K. Yang, and X. Sun, “Precise localization of concealed objects in millimeter-wave images via semantic segmentation,” *IEEE Access*, vol. 8, pp. 121 246–121 256, 2020.
- [205] S. Bakhtiari, S. Liao, T. Elmer, A. Raptis *et al.*, “A real-time heart rate analysis for a remote millimeter wave IQ sensor,” *IEEE Trans. Biomed. Eng.*, vol. 58, no. 6, pp. 1839–1845, 2011.
- [206] J. Lien, N. Gillian, M. E. Karagozler, P. Amihood, C. Schwesig, E. Olson, H. Raja, and I. Poupyrev, “Soli: Ubiquitous gesture sensing with millimeter wave radar,” *ACM Trans. on Graphics*, vol. 35, no. 4, pp. 1–19, 2016.
- [207] C. Xu, Z. Li, H. Zhang, A. S. Rathore, H. Li, C. Song, K. Wang, and W. Xu, “Waveear: Exploring a mmwave-based noise-resistant speech sensing for voice-user interface,” in *Proc. ACM MobiSys*, 2019, pp. 14–26.
- [208] T.-Y. J. Kao, Y. Yan, T.-M. Shen, A. Y.-K. Chen, and J. Lin, “Design and analysis of a 60-GHz CMOS doppler micro-radar system-in-package for vital-sign and vibration detection,” *IEEE Trans. Microw. Theory Techn.*, vol. 61, no. 4, pp. 1649–1659, 2013.